Article

Cell Reports

Spontaneous Pain Disrupts Ventral Hippocampal CA1-Infralimbic Cortex Connectivity and Modulates Pain Progression in Rats with Peripheral Inflammation

Graphical Abstract

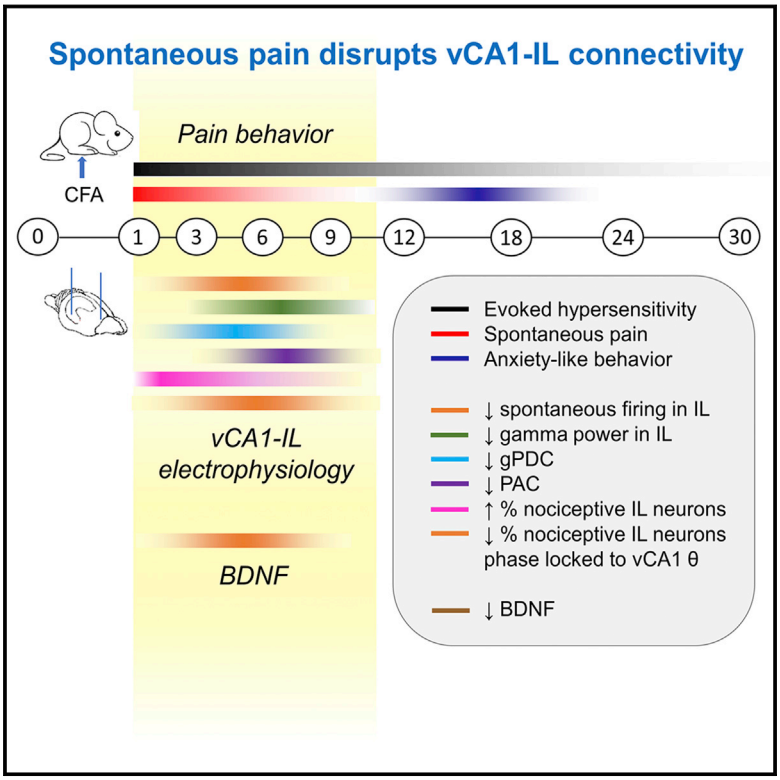

Highlights

- Ventral hippocampal CA1-infralimbic cortex (vCA1-IL) connectivity is involved in pain
- Persistent spontaneous pain in rats with inflammation disrupts vCA1-IL connectivity
- Activating vCA1-IL alleviates spontaneous pain and promotes overall pain recovery
- BDNF expression correlates with behavior and activity changes in spontaneous pain

Authors

Longyu Ma, Lupeng Yue, Yuqi Zhang, ..., Feng-Yu Liu, You Wan, Ming Yi

Correspondence

ywan@hsc.pku.edu.cn (Y.W.), mingyi@hsc.pku.edu.cn (M.Y.)

In Brief

Ma et al. show that persistent spontaneous pain disrupts ventral hippocampal CA1-infralimbic cortex (vCA1-IL) connectivity in rats with peripheral inflammation. Genetic rescue of vCA1-IL dysfunction relieves spontaneous pain and accelerates overall pain recovery. This work identifies a neural pathway that specifically correlates with spontaneous pain.

Ma et al., 2019, Cell Reports *29*, 1579–1593
November 5, 2019
https://doi.org/10.1016/j.celrep.2019.10.002

CellPress

Cell Reports
Article

Spontaneous Pain Disrupts Ventral Hippocampal CA1-Infralimbic Cortex Connectivity and Modulates Pain Progression in Rats with Peripheral Inflammation

Longyu Ma,[1,6] Lupeng Yue,[2,3,6] Yuqi Zhang,[1] Yue Wang,[1] Bingxuan Han,[1] Shuang Cui,[1] Feng-Yu Liu,[1] You Wan,[1,4,5,*] and Ming Yi[1,4,7,*]

[1]Neuroscience Research Institute and Department of Neurobiology, School of Basic Medical Sciences, Peking University, Beijing 100083, P.R. China
[2]CAS Key Laboratory of Mental Health, Institute of Psychology, Beijing 100101, China
[3]Department of Psychology, University of Chinese Academy of Science, Beijing 100101, China
[4]Key Laboratory for Neuroscience, Ministry of Education/National Health Commission, Peking University, Beijing 100083, P.R. China
[5]Co-innovation Center of Neuroregeneration, Nantong University, Nantong 226001, China
[6]These authors contributed equally
[7]Lead Contact
*Correspondence: ywan@hsc.pku.edu.cn (Y.W.), mingyi@hsc.pku.edu.cn (M.Y.)
https://doi.org/10.1016/j.celrep.2019.10.002

SUMMARY

Pain involves an intrinsically dynamic connectome characterized by fluctuating spontaneous brain activity and continuous neuroplastic changes of relevant circuits. Activity in the hippocampus-medial prefrontal cortex (mPFC) pathway has been suggested to correlate with spontaneous pain and pain chronicity, but causal evidence is lacking. Here we combine longitudinal *in vivo* electrophysiological recording with behavioral testing and show that persistent spontaneous pain disrupts ventral hippocampal CA1-infralimbic cortex (vCA1-IL) connectivity and hippocampal modulation of IL neuronal activity in rats with peripheral inflammation. Chemo- and optogenetic rescue of vCA1-IL dysfunction relieves spontaneous pain. Circuit-specific overexpression of brain-derived neurotrophic factor (BDNF) in vCA1-IL reverses electrophysiological changes, relieves spontaneous pain, and accelerates overall recovery from inflammatory pain. Our work identifies a neural pathway that specifically correlates with spontaneous pain and supports the significance of using a circuit dynamics-based strategy for more comprehensive understanding of circuitry mechanisms underlying chronic pain.

INTRODUCTION

Inflammation frequently accompanies injury, surgery, and various diseases. Inflammatory pain is an intrinsically dynamic connectome, showing dynamic changes in spontaneous and evoked brain activity and neuroplasticity of pain-related circuits that correlate with specific pain behaviors (Fillingim et al., 2016). Although acute pain represents a warning signal for tissue injury, chronic pain is debilitating and frequently encompasses multiple behavioral dimensions (Fillingim et al., 2016; Williams and Craig, 2016). Spontaneous pain is a common manifestation of inflammation and has a strong impact on resting brain activity. Persistent spontaneous pain modulates evoked responses to noxious stimuli and negative affect, thus affects overall progression of pain (Baliki et al., 2010). Although evoked pain typically implicates the pain matrix, including somatosensory cortices (Frediani and Bussone, 2019; Garcia-Larrea and Peyron, 2013; Lee et al., 2019), brain correlates of spontaneous pain are poorly defined.

Neuroimaging studies have revealed increasing implication of the limbic system with prolonged duration of pain (Geha et al., 2008; Vachon-Presseau et al., 2016). In particular, the hippocampus-medial prefrontal cortex (mPFC) pathway participates in a variety of behaviors, such as memory (Spellman et al., 2015), goal-directed behavior (Eichenbaum, 2017; Le Merre et al., 2018), and anxiety (Adhikari et al., 2010; Padilla-Coreano et al., 2016), all of which are affected in chronic pain. More recent evidence has demonstrated more direct correlation between the hippocampus-mPFC pathway and pain. Prefrontal activity and hippocampus-mPFC connectivity correlate with the intensity of spontaneous pain (Baliki et al., 2006; Boly et al., 2007), and patients who fail to recover from subacute back pain show larger decreases in hippocampal connectivity with mPFC than those do (Mutso et al., 2014). More intriguingly, patients with lower hippocampus- and mPFC-dependent cognitive functions are at a higher risk to develop post-surgical pain (Attal et al., 2014), whereas lower mPFC-limbic connectivity in the subacute phase predicts transition to chronic pain (Baliki et al., 2012). Both the hippocampus and mPFC are composed of multiple subregions with distinct anatomy, physiology, and functions (Fanselow and Dong, 2010; George and Koob, 2010). In rodents, suppressed dorsal hippocampal activity underlies cognitive deficits in chronic pain (Cardoso-Cruz et al., 2013). By contrast, the ventral hippocampus is more involved in perceptual and affective dimensions of pain (Jiang et al., 2018; Zheng et al., 2017). Efferents from ventral

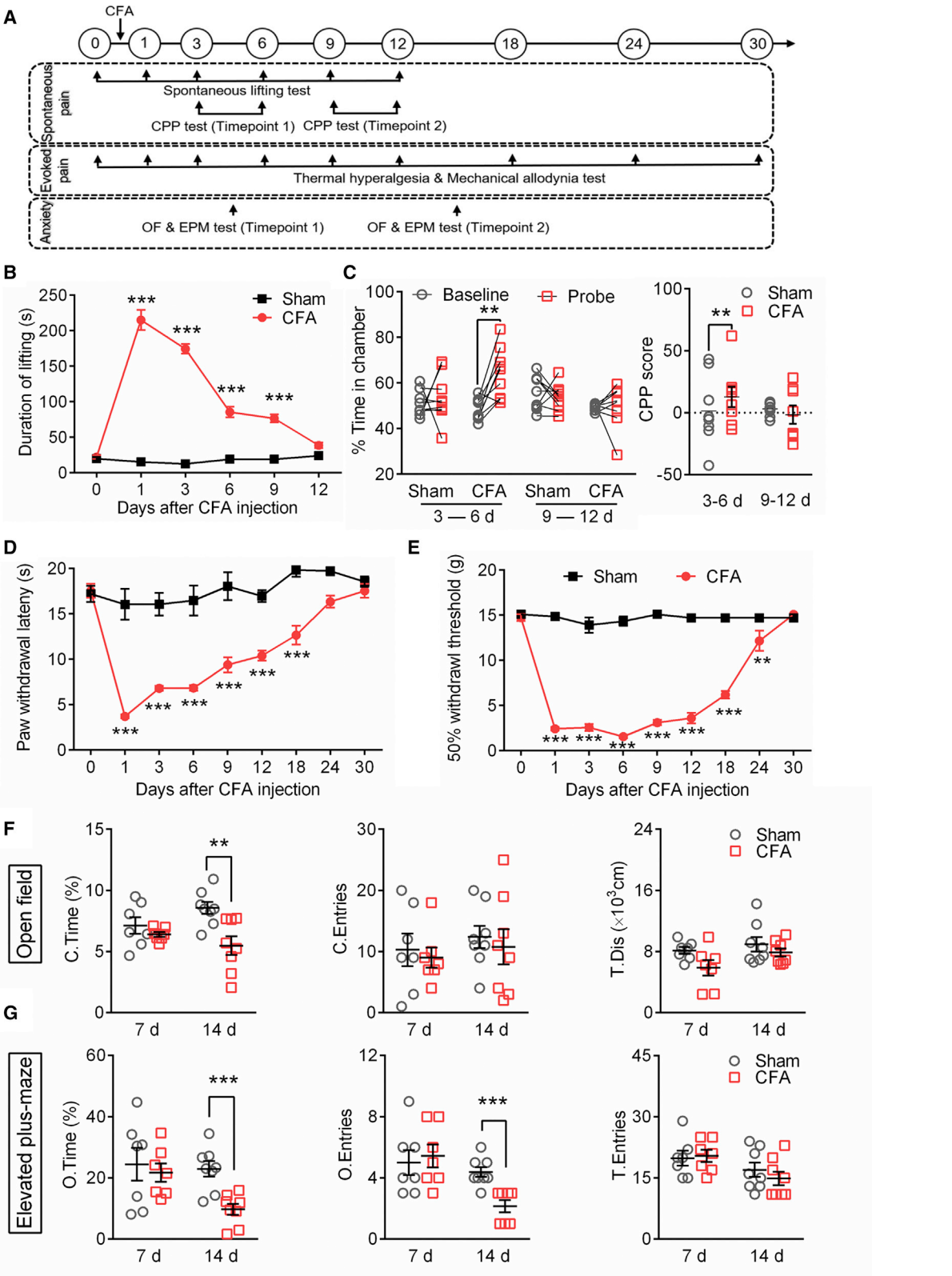

(legend on next page)

hippocampal CA1 (vCA1) pyramidal neurons target pyramidal neurons in the layer V and form excitatory synapses in the infralimbic (IL) subregion of the mPFC (Prasad and Chudasama, 2013; Vertes et al., 2007). Excitability of IL neurons is significantly suppressed in chronic pain (Chu Sin Chung et al., 2017; Ji and Neugebauer, 2014; Kiritoshi et al., 2016).

These lines of evidence consistently indicate the hippocampus-mPFC pathway as an active modulator of spontaneous pain behavior and overall pain chronicity. However, direct evidence for this hypothesis is lacking. With a circuit dynamics-based strategy, we performed longitudinal monitoring of pain behaviors and *in vivo* electrophysiological dynamics followed by genetic intervention and causally verified the role of the vCA1-IL pathway in pain behaviors of rats with peripheral inflammation.

RESULTS

Behavioral Profile of CFA-Induced Inflammatory Pain

We first examined temporal profiles of various pain behaviors in rats with peripheral inflammation induced by intraplantar injection of complete Freund's adjuvant (CFA) (Figure 1A). CFA-induced inflammation induced spontaneous paw lifting, licking, and flinching from day 1 to day 9 and disappeared after day 12 (Figure 1B). These behaviors result from spontaneous firing of C-fiber nociceptors and are indicative of spontaneous pain (Acosta et al., 2014; Djouhri et al., 2006; Matson et al., 2015; Xu et al., 2010). The longitudinal timing of spontaneous pain was further confirmed by conditioned place preference (CPP), indicated by more time spent in the morphine-paired chamber after conditioning during 3–6 days but not 9–12 days post-CFA injection (Figure 1C). By contrast, CFA-induced thermal hyperalgesia (Figure 1D) and mechanical allodynia (Figure 1E) were more persistent and lasted up to ~20 days post-injection. Anxiety-like behavior, a common comorbidity of inflammatory pain (Williams and Craig, 2016), was apparent in a late stage (CFA day 14) but not earlier (CFA day 7), indicated by less time spent in the central area of the open field (Figure 1F) and less time spent and fewer entries into the open arms of the elevated plus maze (Figure 1G). Thus, CFA-induced inflammation is characterized by multiple pain behaviors with distinct temporal profiles.

Spontaneous Pain Disrupts vCA1-IL Connectivity in Rats with Peripheral Inflammation

We monitored longitudinal (before and 1, 3, 6, 9, and 12 days after model establishment) electrophysiological features of the vCA1-IL pathway along the development, maintenance, and recovery of CFA-induced inflammatory pain. A total of 1,269 single units in layer V of the IL, a major prefrontal target of vCA1 efferents (Figure S1), were recorded. Among them, 1,141 were putative pyramidal neurons, on the basis of their waveform and firing properties (Barthó et al., 2004). Putative interneurons were excluded from further analysis considering their low proportion.

Under resting state, we observed lower spontaneous neuronal activity (Figure 2A) and lower power spectral density in the low gamma band (Figure 2B; Figure S2) in the IL, which were apparent on CFA days 3–9 of inflammatory pain. In addition, generalized partial directed coherence (gPDC) revealed decreased information flow from vCA1 to IL but not in the opposite direction between 6 and 12 days after CFA injection (Figures 2C and 2E). Finally, phase-amplitude coupling (PAC) analysis showed clear modulation of gamma (70–90 Hz) amplitudes of the IL by the theta (4–8 Hz) phase of the vCA1, which weakened 6 and 9 days after CFA injection (Figures 3D and 3F; Figure S2).

We further examined nociceptive responses of IL pyramidal neurons to nociceptive laser stimuli in the affected paw (Figure 3A). We observed a remarkably increased proportion of laser-excitatory neurons 1–6 days after CFA injection (Figures 3B and 3C). No changes in the proportion of laser-inhibitory neurons in CFA rats (Figures 3B and 3C) or the proportion of either responsive category in control rats (Figure S3) were detected. The magnitude of neuronal responses remained similar across all phases (Figure 3D). Nociceptive laser stimuli induced stronger theta but weaker gamma power changes in the IL on CFA days 3–9 (Figure S3). Upon nociceptive stimuli, a proportion of IL neurons fired preferentially in specific phases of hippocampal theta oscillation (Figures 4A and 3B), indicating hippocampal modulation of evoked IL neuronal activity. Such modulation was weakened on CFA days 3–9, as we observed significantly lower proportion of IL neurons phase-locked to hippocampal theta upon laser stimuli (Figure 4; Figure S4). Note that none of evoked electrophysiological changes were apparent after CFA day 9, despite persistent evoked nociceptive hypersensitivity (Figures 1D and 1E).

Figure 1. Temporal Variations of Different Pain Behaviors in CFA-Induced Inflammation

(A) Diagram showing the timeline of behavioral tests in five cohorts of animals. Spontaneous paw lifting was examined at baseline (day 0) and 1, 3, 6, 9m and 12 days after modeling (cohort 1). CPP test was performed 3–6 days (cohort 2) or 9–12 days (cohort 3) after modeling. Paw withdrawal latency (PWL) to thermal stimuli and paw withdrawal threshold (PWT) to mechanical stimuli were measured at baseline (day 0) and 1, 3, 6, 9, 12, 18, 24, and 30 days after intraplantar CFA or saline injection (cohort 1). Open field and elevated plus maze tests were performed on days 7 and 8 (cohort 4) or days 12 and 13 (cohort 5) after modeling.

(B) Spontaneous paw lifting, licking, and flinching were apparent 1–9 days after CFA injection. n = 6 per group. ***$p < 0.001$, two-way ANOVA with Bonferroni's post hoc test.

(C) Morphine induced CPP in CFA-treated rats during CFA days 3–6 but not CFA days 9–12. n = 8 or 9 per group. Left: percentage of time spent in morphine-paired chamber before and after conditioning. **$p < 0.01$, paired t test, baseline versus probe. Right: CPP score. *$p < 0.05$, unpaired t test.

(D and E) Thermal hyperalgesia (D) and mechanical allodynia (E) developed in CFA-treated rats. n = 9 per group. Two*$p < 0.05$ and ***$p < 0.001$, two-way ANOVA with Bonferroni's post hoc test.

(F and G) Decreased time spent (left) in the central area of the open field (F) and decreased time spent (left) and entries (middle) into the open arms in the elevated plus maze test (G) in CFA-treated rats 14 days but not 7 days after CFA injection. Total distance and entries (right) remained similar across groups. n = 7 or 8 in each group. **$p < 0.01$ and ***$p < 0.001$, unpaired t test.

Data are represented as mean ± SEM.

See also Tables S1 and S2.

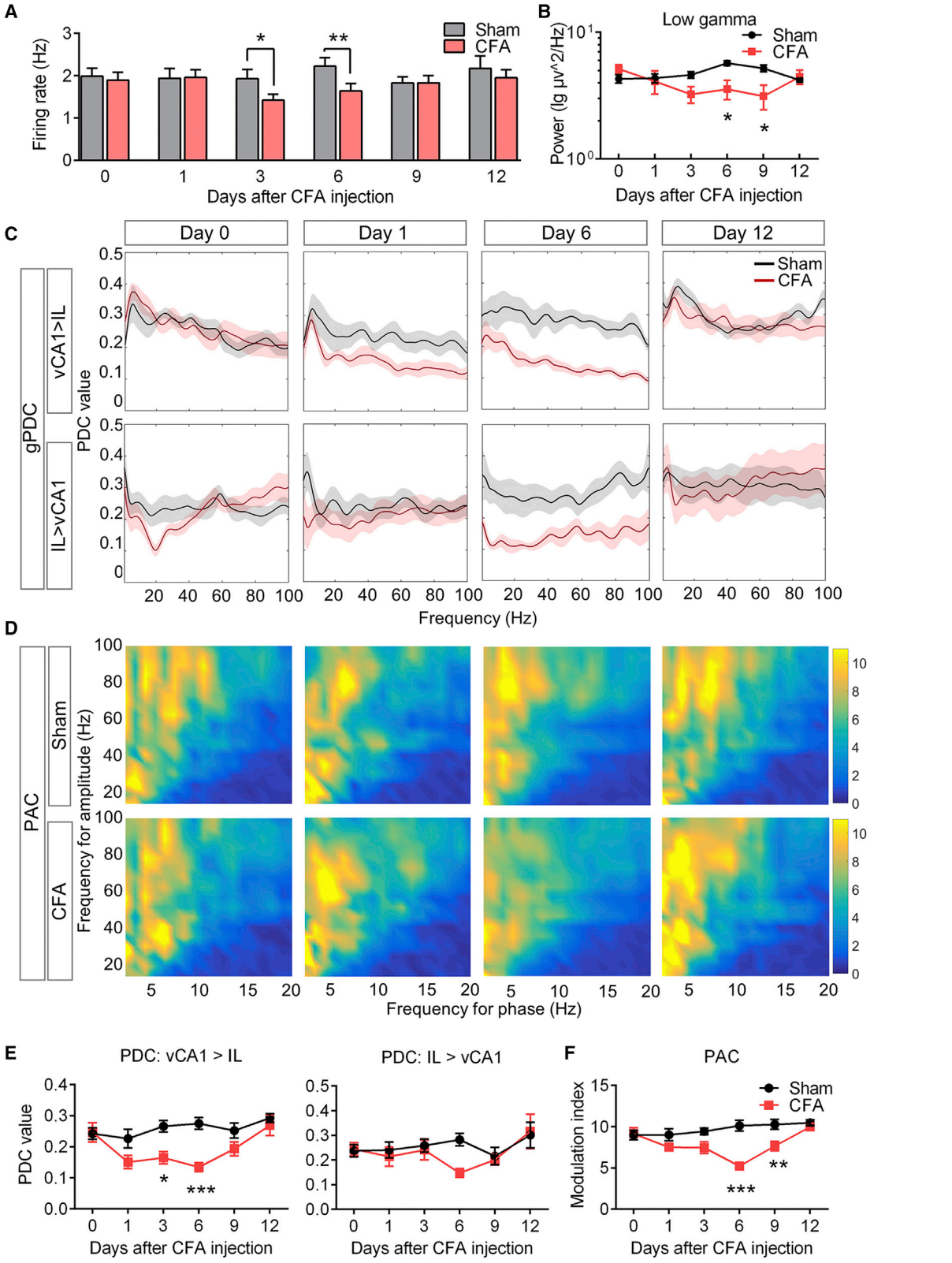

(legend on next page)

Together, electrophysiological changes of the vCA1-IL pathway temporally parallel, with a short delay in initiation, spontaneous pain, but not other pain behaviors (Figure 1), suggesting that persistent spontaneous pain might underlie vCA1-IL dysfunction. Supporting this conclusion, administration of ibuprofen, a commonly used nonsteroidal analgesic, resulted in simultaneous relief of spontaneous pain and reversal of electrophysiological changes of the vCA1-IL pathway in rats with inflammatory pain (Figure 5) but not in normal rats without pain (data not shown). Additional evidence came from the observation that paw lifting and flinching, behavioral indicators of severe spontaneous pain (Acosta et al., 2014; Djouhri et al., 2006; Matson et al., 2015; Xu et al., 2010), were accompanied by more significant changes in vCA1-IL connectivity (Figure S5).

Overall, these findings indicate that spontaneous pain disrupts vCA1-IL connectivity in rats with peripheral inflammation.

Genetic Activation of vCA1-IL Pathway Relieves Spontaneous Pain and Accelerates Overall Recovery from Inflammatory Pain

We next examined whether genetic rescue of vCA1-IL dysfunction would affect pain behavior. We transfected vCA1 pyramidal neurons with the virus containing hM3Dq, an artificially designed receptor selectively activated by a designed drug, clozapine N-oxide (CNO). CNO delivery in the IL activated vCA1 axon terminals (Figures 6A–6D; Figure S6) and produced a sustained increase in the firing rate of IL neurons for more than 8 h (Figure 6E). The vast majority of vCA1 pyramidal neurons project to single target regions (Kim and Cho, 2017), ensuring circuit specificity of the manipulation. Chemogenetic rescue of vCA1-IL pathway remarkably reduced spontaneous paw lifting time following a single dose of CNO on CFA day 3 (Figure 6F) and induced strong preference to the CNO-paired chamber on CFA day 7 after repeated CNO delivery in the IL during CFA days 3–6 in the CPP test (Figure 6G), both indicating relief of spontaneous pain. Similar results were obtained with optogenetic intervention (Figure S6). In contrast, activating the vCA1-IL pathway did not consistently attenuate thermal hyperalgesia in inflammatory pain. Relief of thermal hyperalgesia was apparent only during CFA days 3–9, when both spontaneous pain and vCA1-IL dysfunction (Figures 2, 3, and 4) were present, but not at later time points, when spontaneous pain diminished (Figure S6). Together, these data demonstrate causal links between vCA1-IL dysfunction and spontaneous pain and indicate a significant interaction between spontaneous and evoked pain behaviors (see Discussion).

These findings raised the possibility that long-term vCA1-IL activation would accelerate overall recovery from inflammatory pain. To test this hypothesis, we performed daily CNO microinjection into the IL during CFA days 3–6, when significant alternation of vCA1-IL connectivity was detected. As we expected, this strategy accelerated recovery from thermal hyperalgesia and mechanical allodynia (Figures 6H and 6I) and attenuated anxiety-like behaviors (Figures 6J–6M).

BDNF Deficits Underlie Disrupted vCA1-IL Connectivity in Inflammatory Pain

Brain-derived neurotrophic factor (BDNF) is a crucial molecule for neuroplasticity in the corticolimbic system, including the hippocampus-mPFC pathway (Marosi and Mattson, 2014). We observed downregulated BDNF levels in both vCA1 and IL on day 3 after CFA injection, which reversed on day 9 (Figure 7A). We infused a retro-virus (rAAV2-Cre-GFP) into the IL, which retrograded from axon terminals in the IL to neuronal soma in the vCA1 and allowed BDNF expression in collaboration with Cre-dependent DIO-BDNF-mCherry injected in the vCA1 (Figures 7B and 7C; Figure S7). After viral expression, rats in BDNF and vector groups received CFA injection. vCA1-IL pathway-specific overexpression of BDNF elevated BDNF levels in both regions (Figure 7D) and reversed electrophysiological changes, including lower spontaneous IL neuronal firing (Figure 7E), lower power in the gamma band in the IL (Figure 7F), decreased vCA1-to-IL information flow (Figure 7G), and decreased PAC (Figures 7H and 7I). Behaviorally, BDNF overexpression alleviated spontaneous pain (Figure 7J), thermal hyperalgesia (Figure 7K, left), mechanical allodynia (Figure 7K, right), and anxiety-like behaviors (Figures 7L–7O), indicating accelerated recovery from inflammatory pain. Together, these data suggest that BDNF deficits underlie disrupted vCA1-IL connectivity in inflammatory pain.

DISCUSSION

Spontaneous Pain and vCA1-IL Dynamics

Pain is a network phenomenon involving dynamic interactions among sensory, cognitive, affective, and motivational processes, all of which recruit hippocampus and mPFC. Consistently, neuroimaging studies have revealed chronic pain as an intrinsically dynamic connectome (Kucyi and Davis, 2015). Structural and functional changes of both ventral hippocampus and IL have been reported in chronic pain, but usually at single time points (Apkarian et al., 2011; Garcia-Larrea and Peyron,

Figure 2. Suppressed IL Activity and vCA1-IL Connectivity Temporally Parallels Spontaneous Pain in Rats with Peripheral Inflammation

(A) Decreased spontaneous firing rate of putative IL pyramidal neurons 3 and 6 days after CFA injection. Data from eight rats in each group. *$p < 0.05$ and **$p < 0.01$, Mann-Whitney test.

(B) Decreased local field potential (LFP) power in the low gamma band of the IL on 6 and 9 days after CFA injection. n = 8 per group. *$p < 0.05$, two-way ANOVA with Bonferroni's post hoc test.

(C) Diagrams of gPDC for simultaneously recorded LFPs in IL and vCA1 at baseline (day 0) and 1, 6, and 12 days after CFA injection. Shaded area, SEM.

(D) Standard PAC comodulograms describing the extent of LFP amplitude of the IL (15–100 Hz) modulated by LFP phase of the vCA1 (2–20 Hz) at baseline (day 0) and 1, 6, and 12 days after CFA injection.

(E and F) Quantitative statistics of (A) and (B), respectively. PDC values were averaged across the entire frequency spectrum. Modulation index was calculated by the combination of LFP amplitude of the IL (70–90 Hz) and LFP phase of the vCA1 (4–8 Hz). n = 8 per group. *$p < 0.05$, **$p < 0.01$, and ***$p < 0.001$, two-way ANOVA with Bonferroni's post hoc test.

Data are represented as mean ± SEM. See also Figures S1 and S2 and Tables S1 and S2.

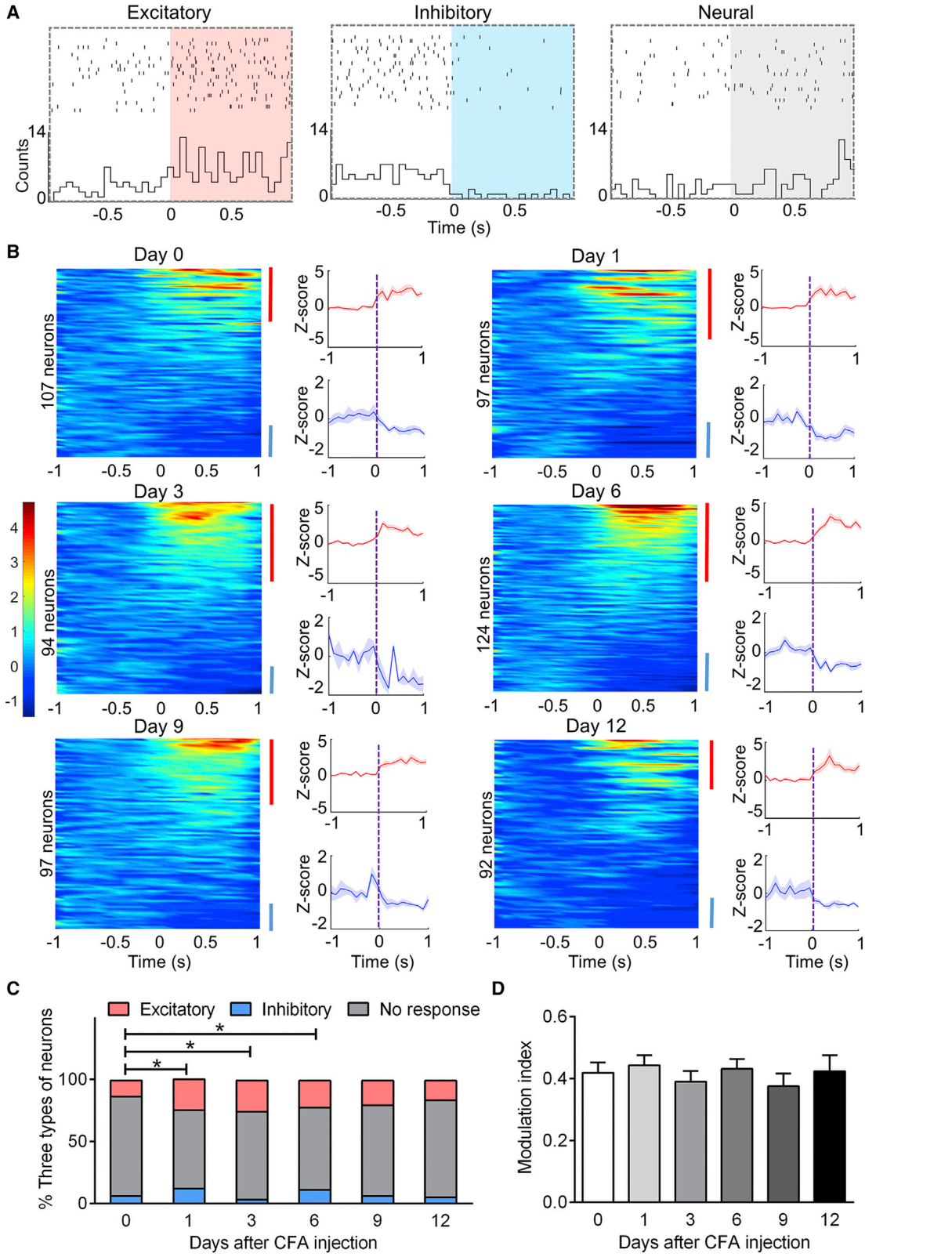

(legend on next page)

2013; Khan et al., 2014; Ong et al., 2019). In the present study, we identified disrupted vCA1-IL connectivity in a specific phase of inflammatory pain characterized by spontaneous pain but no other pain behaviors. Pain studies in animals have long focused on evoked nociceptive responses, until distinct mechanisms between evoked and spontaneous pain are gradually acknowledged (Boly et al., 2007; Samineni et al., 2017; Zain and Bonin, 2019). Indeed, persistent spontaneous pain may exert much stronger influence on resting brain activity than evoked nociception. In the present study, we examined spontaneous paw lifting and CPP, two widely applied paradigms for rodent spontaneous pain. Early studies claim that spontaneous paw-lifting behaviors are present only within 72 h in the CFA model (Djouhri et al., 2006; Lee et al., 2018). However, the observation period in these studies is usually short (5 min). A longer observation time of 30 min confirms 7–9 days' presence of spontaneous pain in the CFA model (Lee et al., 2018), similar to findings in the present study.

Spontaneous pain was significantly attenuated by activating vCA1-IL, representing a functional facet of the vCA1-IL pathway in addition to goal-directed behaviors, memory, and anxiety (Eichenbaum, 2017; Hiser and Koenigs, 2018). One explanation for our findings is that pain relief results indirectly from anxiolysis induced by vCA1-IL activation. vCA1-IL pathway actively regulates spontaneous negative affect including innate anxiety (Abbas et al., 2018; Adhikari et al., 2010; Padilla-Coreano et al., 2016), which may partially underlies the induced conditioned preference in the CPP test. However, we do not consider anxiolysis to be the chief mechanism of analgesia. Transient optogenetic activation is sufficient to induce strong analgesia, including spontaneous paw-lifting behaviors, which more reflect peripheral reflexes (Djouhri et al., 2006). In addition, anxiety-like behaviors are obvious only in chronic inflammatory pain (CFA day 14), much later than the observed period of strong analgesia (days 3–9). Finally, previous work suggests that inhibition of the vCA1-IL pathway, rather than activation, produces anxiolysis (Padilla-Coreano et al., 2016). The descending pathway, which is under modulation of corticolimbic circuits (Kwon et al., 2014), could participate in the pain relief induced by vCA1-IL activation.

Another intriguing finding is the attenuated evoked nociceptive responses with vCA1-IL activation, but only in the period when spontaneous pain is prominent. Neuroimaging has shown that pain-intensity ratings upon nociceptive stimulation positively correlate with baseline fluctuations in the ACC, suggesting that baseline brain activity profoundly modifies evoked pain responses (Boly et al., 2007). This is confirmed by significant differences in stimulus-evoked brain responses in chronic pain: positive phasic nucleus accumbens activation occurs at stimulus offset and predict pain relief in normal subjects but not in patients with chronic pain (Baliki et al., 2010). The gPDC from vCA1 to IL decreased on CFA days 3–6, indicating impaired directional information flow (Baccala et al., 2007). Consistently, reduced phase-locking neurons indicate weakened vCA1 modulation over IL neuronal responses to nociceptive stimuli. These mechanisms could underlie the interaction between spontaneous pain and evoked nociceptive responses and explain the overall pain recovery upon vCA1-IL rescue.

BDNF in the spinal dorsal horn is an active modulator of pain (Merighi et al., 2008). However, in sharp contrast to the spinal cord (Garraway and Huie, 2016), hippocampal and prefrontal levels of BDNF decrease in chronic pain (Yue et al., 2017), indicating distinct pain-modulatory effects of the same molecule in different regions.

Recovery from Chronic Pain: Oblivion or Extinction?

Disrupted vCA1-IL connectivity in inflammatory pain is temporary and disappears within 12 days after model establishment. Does this functional recovery represent "oblivion" of previous pain experience, or a inhibitory learning similar to memory extinction? Available evidence supports the latter. Neuroimaging studies have revealed both reversible and irreversible brain changes in patients recovered from chronic pain, indicating only partial brain recovery (Čeko et al., 2015; Rodriguez-Raecke et al., 2009; Seminowicz et al., 2011). In particular, the PL, another major subregion of the mPFC, displays persistent neuronal hyperexcitability that even outlasts all pain behaviors in the same CFA model (Fan et al., 2018; Wu et al., 2016). PL activity is usually inversely related with IL activity, because pyramidal neurons in layer V of IL inhibit PL pyramidal neurons via local interneurons (Ji and Neugebauer, 2012). These findings raise the possibility that normalized vCA1-IL connectivity acts as an inhibitory signal overlying the hypersensitized PL and contributes to recovery from inflammatory pain.

In the present study we adopted an inflammatory rather than a neuropathic pain model. Inflammation is a common consequence of tissue injury and surgery, precursors of chronic pain and/or post-surgical pain in which suppressed hippocampal-neocortical connectivity and function have been identified as risk factors (Walker et al., 2013). In addition, compared with persistent neuropathic pain, animals show significant recovery

Figure 3. Nociceptive Responses of IL Neurons in Inflammatory Pain

(A) Representative excitatory (left), inhibitory (middle), and neutral (right) responses of layer V neurons in the IL to nociceptive laser stimuli. Raster plots (one trial per row) show recorded spikes, and each peri-stimulus time histogram (PSTH) shows the average firing count across all trials, relative to laser onset (50 ms bins).

(B) Laser-evoked responses of IL neurons at baseline (day 0) and 1, 3, 6, 9, and 12 days after CFA injection. Heatmap rows represent the *Z* score-transformed average PSTH for individual neurons, and columns represent time bins relative to laser onset (50 ms width). Blue and red bars indicate statistically significant laser-responsive units. Plots to the right show the average *Z* score responses for laser-excitatory (top) and laser-inhibitory units (bottom). Shaded area, SEM.

(C) A larger proportion of IL neurons showed excitatory nociceptive responses 1–6 days after CFA injection. Data from eight rats in each group. *$p < 0.05$, chi-square test.

(D) The amplitude of laser-evoked responses in IL neurons remained similar in inflammatory pain. $p > 0.05$, one-way ANOVA.

Data are represented as mean ± SEM.

See also Figure S3 and Tables S1 and S2.

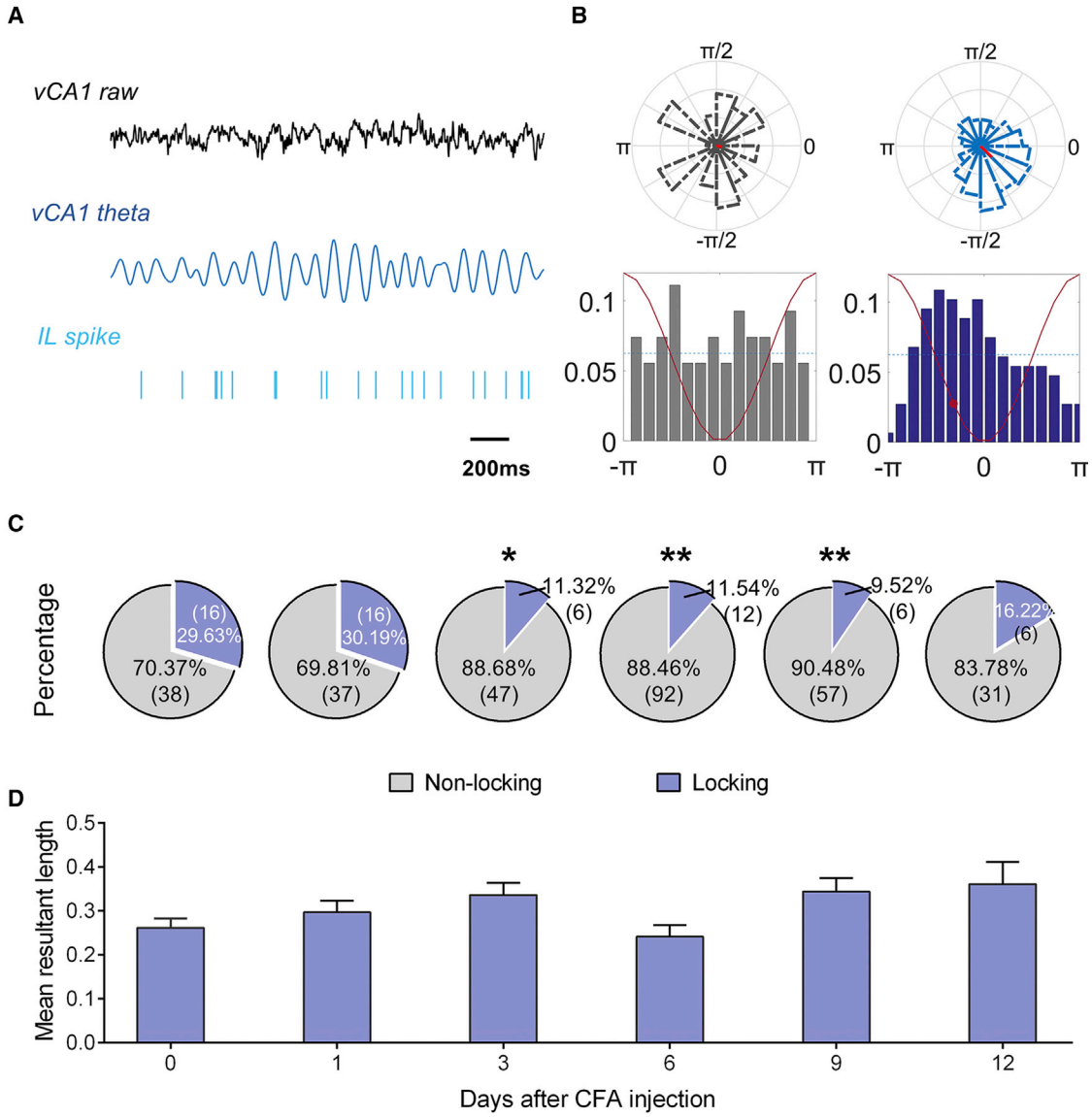

Figure 4. Disrupted Phase Encoding of IL Neurons to vCA1 Theta Oscillation during Inflammatory Pain

(A) Raw vCA1 LFP, band-pass-filtered vCA1 LFP (4–12 Hz), and representative raster plot of IL unit spiking in phase with simultaneously recorded vCA1 theta oscillation.

(B) Examples of a non-phase-locking unit (left) and a phase-locking unit (right) in the IL relative to vCA1 theta oscillation. Radar chart represents Rayleigh test standard (top). Histogram showing the distribution of mean spike theta-phase angles (16 bins per cycle, down). Red line, one schematic theta cycle; red circle, preference phase angle. Left: a non-phase-locking spike with uniform distribution; right: a phase-locking spike with a large deviation of the resulting distribution.

(C) Ratio of putative IL pyramidal neurons locked to vCA1 theta phase during laser-evoked nociceptive responses at different stages of inflammatory pain. The proportion of laser-evoked phase-locking neurons in the IL decreased on CFA days 3–9 compared with baseline. Data from eight rats in each group. *$p < 0.05$ and **$p < 0.01$, chi-square test.

(D) Similar strength of phase-locking in IL neurons coupled to vCA1 theta phase in inflammatory pain. $p = 0.0539$, one-way ANOVA.

Data are represented as mean ± SEM.

See also Figure S4 and Tables S1 and S2.

from inflammatory pain, allowing the evaluation of hippocampal-neocortical contribution to different stages of pain initiation, development, and recovery. Finally, spontaneous pain usually shares a similar temporal profile with evoked pain in neuropathic pain models (King et al., 2009), and their intimate interactions make it difficult to differentiate between these two pain behaviors (King et al., 2011; Tappe-Theodor and Kuner, 2014). But it remains intriguing to extend the present findings to chronic neuropathic pain, which is mechanistically distinct from inflammatory pain and more resistant to clinical treatment.

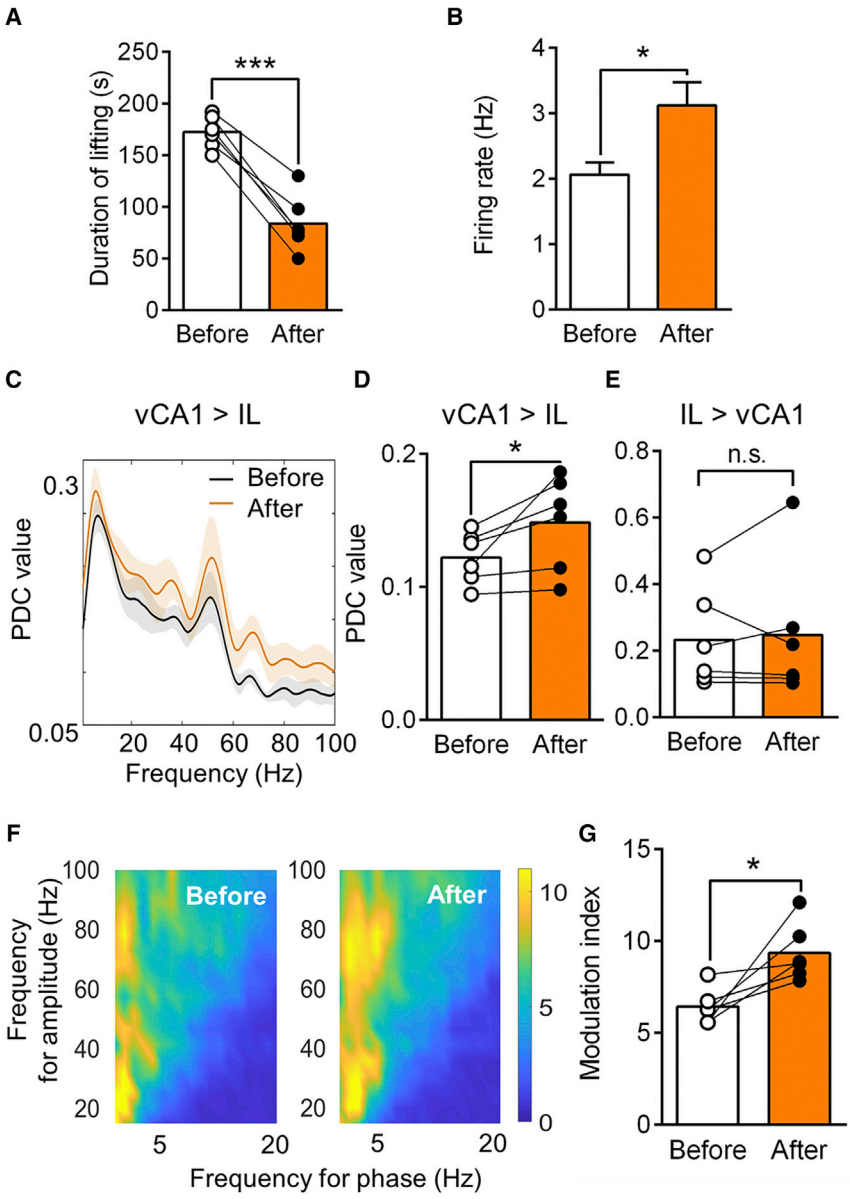

Figure 5. Ibuprofen Alleviates Spontaneous Pain and Reverses Electrophysiological Changes of the vCA1-IL Pathway

(A) Administration of ibuprofen on CFA day 3 alleviated spontaneous paw lifting behavior. n = 6. ***p < 0.001, paired t test.

(B) Administration of ibuprofen increased spontaneous firing rates of IL pyramidal neurons. Data from six rats. *p < 0.05, Mann-Whitney test.

(C) Diagram of gPDC from vCA1 to IL before and after administration of ibuprofen. Data from six rats. Shaded area, SEM.

(D and E) Administration of ibuprofen increased gPDC from vCA1 to IL (D) but not in the opposite direction (E). Data from six rats. *p < 0.05, paired t test.

(F) Standard PAC comodulograms describing the extent of LFP amplitude of the IL (15–100 Hz) modulated by the LFP phase of vCA1 (2–20 Hz) before (left) and after (right) administration of Ibuprofen. Data from six rats.

(G) Administration of ibuprofen increased PAC. Data from six rats. *p < 0.05, paired t test.

Data are represented as mean ± SEM.

See also Figure S5 and Tables S1 and S2.

Clinical Considerations

Current clinical classification of acute, subacute, and chronic pain is arbitrary and based simply on pain duration. Although phasic painful stimulation induces gamma oscillations over brain areas encoding sensory processes, tonic pain shifts these changes to mPFC (Nickel et al., 2017; Schulz et al., 2015). These findings, together with our data, consistently indicate that pain persistence induces a shift of pain-encoding strategy from sensory cortices to emotional-motivational brain areas (Hashmi et al., 2013) and further suggest that certain electrophysiological features may serve to mechanistically differentiate these phases.

Lower mPFC-limbic connectivity in the subacute phase predicts transition to chronic pain (Baliki et al., 2012), whereas cognitive decline increases the risk for post-surgical pain (Attal et al., 2014). Our findings provide clues for the unexpected role of the hippocampal system in pain modulation and put forward a strategy to identify patients at risk for developing chronic pain when they are in the subacute phase or before surgery. Early intervention with analgesics or cognitive behavioral therapy in these patients may help reduce the incidence of chronic or post-surgical pain.

Finally, environmental enrichment alleviates established inflammatory and neuropathic pain in rodents, at least partially through promoting hippocampal functions (Zheng et al., 2017). Many clinically applied analgesics and non-drug pain treatment such as cognitive behavioral therapies, acupuncture, noninvasive electrical stimulation, and dietary interventions, affect hippocampal neurogenesis and functions (Heberden, 2016; Kobelt et al., 2014; Lledo et al., 2006; Nam et al., 2015). Among these non-drug therapies, neuromodulation, including transcranial magnetic/current stimulation, is under active investigation (Graff-Guerrero et al., 2005; Stagg et al., 2013). mPFC may be an ideal target for such modulation, given its easily accessible localization and abundant anatomical interconnection with other pain-modulatory areas (Cheriyan and Sheets, 2018). Our findings provide a mechanistic basis for these therapies and suggest that combined pharmacological therapeutics with non-pharmacological paradigms could be of clinical significance.

Together, the present study reveals that spontaneous pain disrupts vCA1-IL connectivity and modulates pain chronicity in rats with peripheral inflammation and supports the significance of using a circuit dynamics-based strategy for more

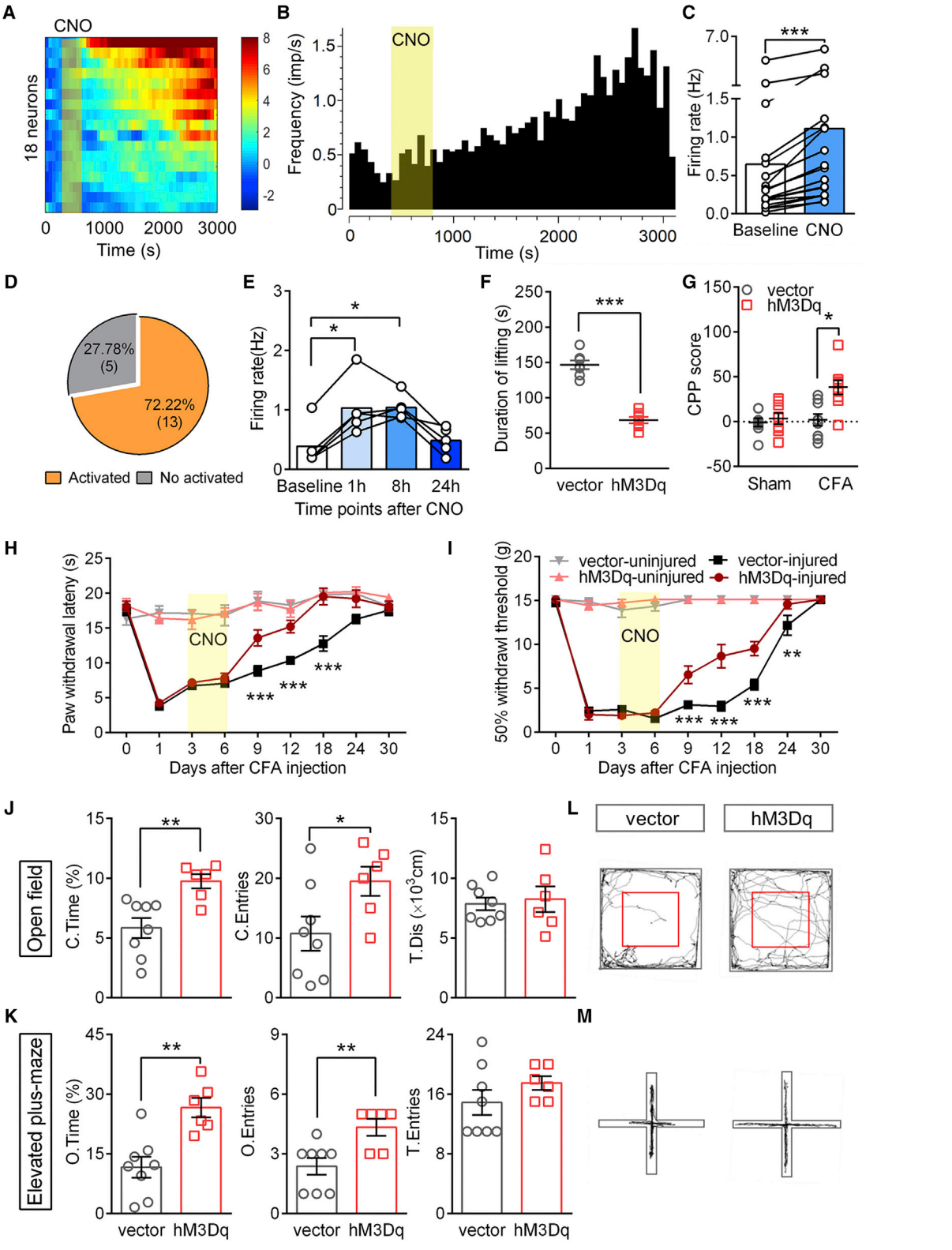

(legend on next page)

comprehensive understanding of central mechanisms underlying chronic pain.

STAR★METHODS

Detailed methods are provided in the online version of this paper and include the following:

- KEY RESOURCES TABLE
- LEAD CONTACT AND MATERIALS AVAILABILITY
- EXPERIMENTAL MODEL AND SUBJECT DETAILS
  - Animals
  - CFA-induced inflammatory pain
- METHOD DETAILS
  - *In vivo* electrophysiology: surgery
  - *In vivo* electrophysiology: recording
  - Electrophysiological data analysis: data preprocessing
  - Electrophysiological data analysis: spike classification
  - Electrophysiological data analysis: power spectral density
  - Electrophysiological data analysis: partial directed coherence
  - Electrophysiological data analysis: phase amplitude coherence
  - Electrophysiological data analysis: spectrogram
  - Electrophysiological data analysis: neuronal response to laser stimuli
  - Electrophysiological data analysis: phase locking
  - Behavioral test: spontaneous paw lifting
  - Behavioral test: conditioned place preference (CPP)
  - Behavioral test: evoked nociceptive responses
  - Behavioral test: open field test
  - Behavioral test: elevated plus-maze test
  - Optogenetics
  - Chemogenetics
  - BDNF overexpression
  - Histology
  - ELISA for BDNF measurement
- QUANTIFICATION AND STATISTICAL ANALYSIS
- DATA AND CODE AVAILABILITY

SUPPLEMENTAL INFORMATION

Supplemental Information can be found online at https://doi.org/10.1016/j.celrep.2019.10.002.

ACKNOWLEDGMENTS

We thank members of the Wan and Yi labs for technical support and helpful suggestions. This work is supported by the National Basic Research Program of the Ministry of Science and Technology of China (2014CB548200 and 2015CB554503), the National Natural Science Foundation of China (91732107, 81571067, 81521063, 31872774, and 81974166), the Beijing Natural Science Foundation (5182013), Key Project of the Chinese Ministry of Education (109003) and the "111" Project of the Ministry of Education of China (B07001). The funders have no role in experimental design, data collection, discussion, or explanation.

AUTHOR CONTRIBUTIONS

Conceptualization, L.M., L.Y., Y.Wan, and M.Y.; Methodology, L.M., L.Y., S.C., F.-Y.L., Y.Wang, and M.Y.; Software, L.Y.; Formal Analysis, L.M. and L.Y.; Investigation, L.M., Y.Z., Y.Wang, and B.H.; Writing – Original Draft, L.M., L.Y., and M.Y.; Writing – Review and Editing, Y.Wan and M.Y.; Visualization, L.M., L.Y., and M.Y.; Funding Acquisition, Y.Wan and M.Y.; Supervision, Y.Wan and M.Y.

DECLARATION OF INTERESTS

The authors declare no competing interests.

Received: April 10, 2019
Revised: September 2, 2019
Accepted: October 1, 2019
Published: November 5, 2019

Figure 6. Long-Term Chemogenetic Activation of vCA1-IL Pathway Alleviates Spontaneous Pain, Thermal Hyperalgesia, Mechanical Allodynia, and Anxiety-like Behaviors in Rats with Inflammatory Pain

(A) Chemogenetic activation of vCA1-IL pathway increased neuronal activity in the IL. Heatmap rows represent the *Z* score-transformed average PSTH for individual IL neurons, and columns represent time bins relative to recording onset (60 s width). Yellow bar indicates the duration of CNO application.

(B) A representative *in vivo* rate histogram plot showing enhanced activity of a putative pyramidal neuron in the IL upon CNO application in the vicinity of hM3Dq-expressing vCA1 terminals.

(C) Increased mean firing rate of IL neurons following administration of CNO. n = 18 units. ***$p < 0.001$, Wilcoxon signed-rank test.

(D) CNO delivery in the IL increased the firing rate of 72% putative pyramidal neurons in the IL of animals with hM3Dq expression in vCA1, revealed by *in vivo* recording. n = 18 units.

(E) Sustained increase in mean firing rate of IL neurons after CNO delivery. n = 5 per group. *$p < 0.05$, Friedman test with Dunn's post hoc test.

(F) Relieved paw lifting and flinching following a single dose of CNO on CFA day 3. n = 7 per group. ***$p < 0.001$, unpaired t test.

(G) Activation of vCA1-IL pathway on CFA days 3–6 induced preference to the paired chamber in the probe test on CFA day 7 in CFA but not sham rats. n = 9 per group. *$p < 0.05$, unpaired t test.

(H and I) Continuous CNO delivery on CFA days 3–7 accelerated recovery from thermal hyperalgesia (H) and mechanical allodynia (I) in inflammatory pain. n = 9 per group. **$p < 0.01$ and ***$p < 0.001$, two-way ANOVA with Bonferroni's post hoc test.

(J) Long-term activation of vCA1-IL pathway attenuated pain-induced anxiety-like behavior in the open field test on CFA day 14. Chronic pain decreased the time spent (left) and distance traveled (middle) in the central area of the open field, which were reversed by activating vCA1-IL pathway. Total distance traveled (right) in the field was not affected. n = 6–8 per group. *$p < 0.05$ and **$p < 0.01$, unpaired t test.

(K) Activation of vCA1-IL pathway attenuated pain-induced anxiety-like behavior in the elevated plus maze test on CFA day 15. Chronic pain decreased the time spent (left) and entries (middle) of the open arm, which were reversed by activation of pathway. Total arm entries (right) was not significantly different. n = 6–8 per group. **$p < 0.01$, unpaired t test.

(L and M) Representative movement tracks in the open field (L) and the elevated plus maze (M) from rats in control (left) and rescue (right) groups.

Data are represented as mean ± SEM.

See also Figure S6 and Tables S1 and S2.

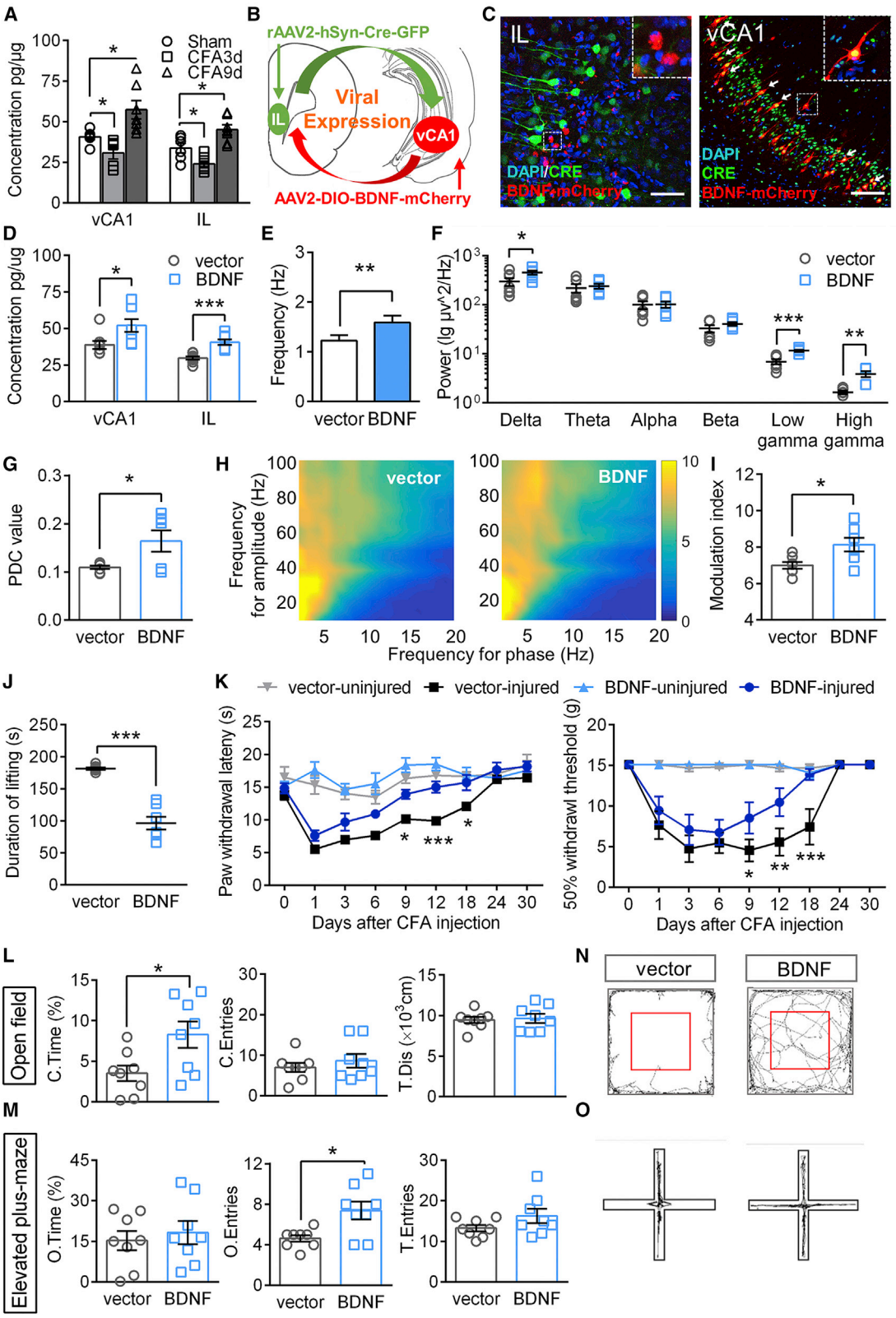

(legend on next page)

REFERENCES

Abbas, A.I., Sundiang, M.J.M., Henoch, B., Morton, M.P., Bolkan, S.S., Park, A.J., Harris, A.Z., Kellendonk, C., and Gordon, J.A. (2018). Somatostatin interneurons facilitate hippocampal-prefrontal synchrony and prefrontal spatial encoding. Neuron *100*, 926–939.e3.

Acosta, C., Djouhri, L., Watkins, R., Berry, C., Bromage, K., and Lawson, S.N. (2014). TREK2 expressed selectively in IB4-binding C-fiber nociceptors hyperpolarizes their membrane potentials and limits spontaneous pain. J. Neurosci. *34*, 1494–1509.

Adhikari, A., Topiwala, M.A., and Gordon, J.A. (2010). Synchronized activity between the ventral hippocampus and the medial prefrontal cortex during anxiety. Neuron *65*, 257–269.

Apkarian, A.V., Hashmi, J.A., and Baliki, M.N. (2011). Pain and the brain: specificity and plasticity of the brain in clinical chronic pain. Pain *152* (*3, Suppl*), S49–S64.

Attal, N., Masselin-Dubois, A., Martinez, V., Jayr, C., Albi, A., Fermanian, J., Bouhassira, D., and Baudic, S. (2014). Does cognitive functioning predict chronic pain? Results from a prospective surgical cohort. Brain *137*, 904–917.

Baccalá, L.A., and Sameshima, K. (2001). Partial directed coherence: a new concept in neural structure determination. Biol. Cybern. *84*, 463–474.

Baccala, L.A., Sameshima, K., and Takahashi, D.Y. (2007). Generalized partial directed coherence. In 15th International Conference on Digital Signal Processing (IEEE), pp. 163–166.

Baliki, M.N., Chialvo, D.R., Geha, P.Y., Levy, R.M., Harden, R.N., Parrish, T.B., and Apkarian, A.V. (2006). Chronic pain and the emotional brain: specific brain activity associated with spontaneous fluctuations of intensity of chronic back pain. J. Neurosci. *26*, 12165–12173.

Baliki, M.N., Geha, P.Y., Fields, H.L., and Apkarian, A.V. (2010). Predicting value of pain and analgesia: nucleus accumbens response to noxious stimuli changes in the presence of chronic pain. Neuron *66*, 149–160.

Baliki, M.N., Petre, B., Torbey, S., Herrmann, K.M., Huang, L., Schnitzer, T.J., Fields, H.L., and Apkarian, A.V. (2012). Corticostriatal functional connectivity predicts transition to chronic back pain. Nat. Neurosci. *15*, 1117–1119.

Barthó, P., Hirase, H., Monconduit, L., Zugaro, M., Harris, K.D., and Buzsáki, G. (2004). Characterization of neocortical principal cells and interneurons by network interactions and extracellular features. J. Neurophysiol. *92*, 600–608.

Boly, M., Balteau, E., Schnakers, C., Degueldre, C., Moonen, G., Luxen, A., Phillips, C., Peigneux, P., Maquet, P., and Laureys, S. (2007). Baseline brain activity fluctuations predict somatosensory perception in humans. Proc. Natl. Acad. Sci. U S A *104*, 12187–12192.

Canolty, R.T., Edwards, E., Dalal, S.S., Soltani, M., Nagarajan, S.S., Kirsch, H.E., Berger, M.S., Barbaro, N.M., and Knight, R.T. (2006). High gamma power is phase-locked to theta oscillations in human neocortex. Science *313*, 1626–1628.

Cardoso-Cruz, H., Lima, D., and Galhardo, V. (2013). Impaired spatial memory performance in a rat model of neuropathic pain is associated with reduced hippocampus-prefrontal cortex connectivity. J. Neurosci. *33*, 2465–2480.

Čeko, M., Shir, Y., Ouellet, J.A., Ware, M.A., Stone, L.S., and Seminowicz, D.A. (2015). Partial recovery of abnormal insula and dorsolateral prefrontal connectivity to cognitive networks in chronic low back pain after treatment. Hum. Brain Mapp. *36*, 2075–2092.

Cheriyan, J., and Sheets, P.L. (2018). Altered excitability and local connectivity of mPFC-PAG neurons in a mouse model of neuropathic pain. J. Neurosci. *38*, 4829–4839.

Chu Sin Chung, P., Panigada, T., Cardis, R., Decosterd, I., and Gosselin, R.D. (2017). Peripheral nerve injury induces a transitory microglial reaction in the rat infralimbic cortex. Neurosci. Lett. *655*, 14–20.

Djouhri, L., Koutsikou, S., Fang, X., McMullan, S., and Lawson, S.N. (2006). Spontaneous pain, both neuropathic and inflammatory, is related to frequency of spontaneous firing in intact C-fiber nociceptors. J. Neurosci. *26*, 1281–1292.

Eichenbaum, H. (2017). Prefrontal-hippocampal interactions in episodic memory. Nat. Rev. Neurosci. *18*, 547–558.

Fan, X.C., Fu, S., Liu, F.Y., Cui, S., Yi, M., and Wan, Y. (2018). Hypersensitivity of prelimbic cortex neurons contributes to aggravated nociceptive responses in rats with experience of chronic inflammatory pain. Front. Mol. Neurosci. *11*, 85.

Fanselow, M.S., and Dong, H.W. (2010). Are the dorsal and ventral hippocampus functionally distinct structures? Neuron *65*, 7–19.

Fillingim, R.B., Loeser, J.D., Baron, R., and Edwards, R.R. (2016). Assessment of chronic pain: domains, methods, and mechanisms. J. Pain *17* (*9, Suppl*), T10–T20.

Frediani, F., and Bussone, G. (2019). When does the brain choose pain? Neurol. Sci. *40* (*Suppl 1*), 27–29.

Garcia-Larrea, L., and Peyron, R. (2013). Pain matrices and neuropathic pain matrices: a review. Pain *154* (*Suppl 1*), S29–S43.

Garraway, S.M., and Huie, J.R. (2016). Spinal plasticity and behavior: BDNF-induced neuromodulation in uninjured and injured spinal cord. Neural Plast. *2016*, 9857201.

Geha, P.Y., Baliki, M.N., Harden, R.N., Bauer, W.R., Parrish, T.B., and Apkarian, A.V. (2008). The brain in chronic CRPS pain: abnormal gray-white matter interactions in emotional and autonomic regions. Neuron *60*, 570–581.

Figure 7. BDNF Deficits Underlie vCA1-IL Dysfunction and Inflammatory Pain

(A) BDNF levels in vCA1 and IL decreased on day 3 but reversed on day 9 after CFA modeling. n = 5–7 per group. *p < 0.05, one-way ANOVA with Bonferroni's post hoc test.

(B) Schematic diagram of BDNF overexpression in the vCA1-IL pathway.

(C) Representative immunofluorescence images showing BDNF-mCherry expression in axonal terminals in the IL (left; scale bar: 50 μm) and co-labeling of the majority of BDNF-mCherry$^+$ neurons (red) with Cre$^+$ neurons (green) (right; scale bar: 100 μm).

(D) Increased BDNF levels in vCA1 and IL after virus expression. n = 8 per group. *p < 0.05 and ***p < 0.001, unpaired t test.

(E and F) BDNF overexpression increased spontaneous firing rates of IL pyramidal neurons (E) and power spectral density of IL in delta, low gamma, and high gamma bands (F) on CFA days 3–6. n = 7 rats per group. **p < 0.01, Mann-Whitney test. *p < 0.05, **p < 0.01, and ***p < 0.001, unpaired t test.

(G) BDNF overexpression increased gPDC from vCA1 to IL on CFA days 3–6. n = 7 per group. *p < 0.05, unpaired t test.

(H) Standard PAC comodulograms describing the extent of LFP amplitude of IL (15–100 Hz) modulated by the LFP phase of vCA1 (2–20 Hz) in control (left) and BDNF overexpression groups (right).

(I) BDNF overexpression elevated the coupling between vCA1 theta phase and IL gamma amplitude on CFA days 3–6. n = 7 per group. *p < 0.05, unpaired t test.

(J) BDNF overexpression reduced the duration of spontaneous lifting and flinching on CFA day 3. n = 8 per group. ***p < 0.001, unpaired t test.

(K) BDNF overexpression attenuated thermal hyperalgesia (left) and mechanical allodynia (right) in inflammatory pain. n = 8 per group. *p < 0.05, **p < 0.01, and ***p < 0.001, two-way ANOVA with Bonferroni's post hoc test.

(L and M) BDNF overexpression reversed chronic pain-induced anxiety-like behaviors in open field (L) and elevated plus maze (M) tests on CFA days 14 and 15. n = 8 per group. *p < 0.05, unpaired t test.

(N and O) Representative movement tracks in the open field (N) and the elevated plus maze (O) from rats in control (left) and BDNF overexpression (right) groups. Data are represented as mean ± SEM.

See also Figure S7 and Tables S1 and S2.

George, O., and Koob, G.F. (2010). Individual differences in prefrontal cortex function and the transition from drug use to drug dependence. Neurosci. Biobehav. Rev. *35*, 232–247.

Graff-Guerrero, A., González-Olvera, J., Fresán, A., Gómez-Martín, D., Méndez-Núñez, J.C., and Pellicer, F. (2005). Repetitive transcranial magnetic stimulation of dorsolateral prefrontal cortex increases tolerance to human experimental pain. Brain Res. Cogn. Brain Res. *25*, 153–160.

Hashmi, J.A., Baliki, M.N., Huang, L., Baria, A.T., Torbey, S., Hermann, K.M., Schnitzer, T.J., and Apkarian, A.V. (2013). Shape shifting pain: chronification of back pain shifts brain representation from nociceptive to emotional circuits. Brain *136*, 2751–2768.

Heberden, C. (2016). Modulating adult neurogenesis through dietary interventions. Nutr. Res. Rev. *29*, 163–171.

Hiser, J., and Koenigs, M. (2018). The multifaceted role of the ventromedial prefrontal cortex in emotion, decision making, social cognition, and psychopathology. Biol. Psychiatry *83*, 638–647.

Hung, C.H., Wang, J.C., and Strichartz, G.R. (2015). Spontaneous chronic pain after experimental thoracotomy revealed by conditioned place preference: morphine differentiates tactile evoked pain from spontaneous pain. J. Pain *16*, 903–912.

Ji, G., and Neugebauer, V. (2012). Modulation of medial prefrontal cortical activity using in vivo recordings and optogenetics. Mol. Brain *5*, 36.

Ji, G., and Neugebauer, V. (2014). CB1 augments mGluR5 function in medial prefrontal cortical neurons to inhibit amygdala hyperactivity in an arthritis pain model. Eur. J. Neurosci. *39*, 455–466.

Jiang, Y.Y., Shao, S., Zhang, Y., Zheng, J., Chen, X., Cui, S., Liu, F.Y., Wan, Y., and Yi, M. (2018). Neural pathways in medial septal cholinergic modulation of chronic pain: distinct contribution of the anterior cingulate cortex and ventral hippocampus. Pain *159*, 1550–1561.

Khan, S.A., Keaser, M.L., Meiller, T.F., and Seminowicz, D.A. (2014). Altered structure and function in the hippocampus and medial prefrontal cortex in patients with burning mouth syndrome. Pain *155*, 1472–1480.

Kim, W.B., and Cho, J.H. (2017). Synaptic targeting of double-projecting ventral CA1 hippocampal neurons to the medial prefrontal cortex and basal amygdala. J. Neurosci. *37*, 4868–4882.

King, T., Vera-Portocarrero, L., Gutierrez, T., Vanderah, T.W., Dussor, G., Lai, J., Fields, H.L., and Porreca, F. (2009). Unmasking the tonic-aversive state in neuropathic pain. Nat. Neurosci. *12*, 1364–1366.

King, T., Qu, C., Okun, A., Mercado, R., Ren, J., Brion, T., Lai, J., and Porreca, F. (2011). Contribution of afferent pathways to nerve injury-induced spontaneous pain and evoked hypersensitivity. Pain *152*, 1997–2005.

Kiritoshi, T., Ji, G., and Neugebauer, V. (2016). Rescue of impaired mGluR5-driven endocannabinoid signaling restores prefrontal cortical output to inhibit pain in arthritic rats. J. Neurosci. *36*, 837–850.

Kobelt, L.J., Wilkinson, A.E., McCormick, A.M., Willits, R.K., and Leipzig, N.D. (2014). Short duration electrical stimulation to enhance neurite outgrowth and maturation of adult neural stem progenitor cells. Ann. Biomed. Eng. *42*, 2164–2176.

Kucyi, A., and Davis, K.D. (2015). The dynamic pain connectome. Trends Neurosci. *38*, 86–95.

Kwon, M., Altin, M., Duenas, H., and Alev, L. (2014). The role of descending inhibitory pathways on chronic pain modulation and clinical implications. Pain Pract. *14*, 656–667.

Le Merre, P., Esmaeili, V., Charrière, E., Galan, K., Salin, P.A., Petersen, C.C.H., and Crochet, S. (2018). Reward-based learning drives rapid sensory signals in medial prefrontal cortex and dorsal hippocampus necessary for goal-directed behavior. Neuron *97*, 83–91.e5.

LeBlanc, B.W., Lii, T.R., Huang, J.J., Chao, Y.C., Bowary, P.M., Cross, B.S., Lee, M.S., Vera-Portocarrero, L.P., and Saab, C.Y. (2016). T-type calcium channel blocker Z944 restores cortical synchrony and thalamocortical connectivity in a rat model of neuropathic pain. Pain *157*, 255–263.

Lee, P.R., Yoon, S.Y., Kim, H.W., Yeo, J.H., Kim, Y.H., and Oh, S.B. (2018). Peripheral $GABA_A$ receptor-mediated signaling facilitates persistent inflammatory hypersensitivity. Neuropharmacology *135*, 572–580.

Lee, M.J., Park, B.Y., Cho, S., Kim, S.T., Park, H., and Chung, C.S. (2019). Increased connectivity of pain matrix in chronic migraine: a resting-state functional MRI study. J. Headache Pain *20*, 29.

Lledo, P.M., Alonso, M., and Grubb, M.S. (2006). Adult neurogenesis and functional plasticity in neuronal circuits. Nat. Rev. Neurosci. *7*, 179–193.

Mahler, S.V., Vazey, E.M., Beckley, J.T., Keistler, C.R., McGlinchey, E.M., Kaufling, J., Wilson, S.P., Deisseroth, K., Woodward, J.J., and Aston-Jones, G. (2014). Designer receptors show role for ventral pallidum input to ventral tegmental area in cocaine seeking. Nat. Neurosci. *17*, 577–585.

Marosi, K., and Mattson, M.P. (2014). BDNF mediates adaptive brain and body responses to energetic challenges. Trends Endocrinol. Metab. *25*, 89–98.

Matson, D.J., Hamamoto, D.T., Bregman, H., Cooke, M., DiMauro, E.F., Huang, L., Johnson, D., Li, X., McDermott, J., Morgan, C., et al. (2015). Inhibition of inactive states of tetrodotoxin-sensitive sodium channels reduces spontaneous firing of C-fiber nociceptors and produces analgesia in formalin and complete Freund's adjuvant models of pain. PLoS ONE *10*, e0138140.

Merighi, A., Salio, C., Ghirri, A., Lossi, L., Ferrini, F., Betelli, C., and Bardoni, R. (2008). BDNF as a pain modulator. Prog. Neurobiol. *85*, 297–317.

Mutso, A.A., Petre, B., Huang, L., Baliki, M.N., Torbey, S., Herrmann, K.M., Schnitzer, T.J., and Apkarian, A.V. (2014). Reorganization of hippocampal functional connectivity with transition to chronic back pain. J. Neurophysiol. *111*, 1065–1076.

Nam, M.H., Ahn, K.S., and Choi, S.H. (2015). Acupuncture: a potent therapeutic tool for inducing adult neurogenesis. Neural Regen. Res. *10*, 33–35.

Nickel, M.M., May, E.S., Tiemann, L., Schmidt, P., Postorino, M., Ta Dinh, S., Gross, J., and Ploner, M. (2017). Brain oscillations differentially encode noxious stimulus intensity and pain intensity. Neuroimage *148*, 141–147.

Ong, W.Y., Stohler, C.S., and Herr, D.R. (2019). Role of the prefrontal cortex in pain processing. Mol. Neurobiol. *56*, 1137–1166.

Padilla-Coreano, N., Bolkan, S.S., Pierce, G.M., Blackman, D.R., Hardin, W.D., Garcia-Garcia, A.L., Spellman, T.J., and Gordon, J.A. (2016). Direct ventral hippocampal-prefrontal input is required for anxiety-related neural activity and behavior. Neuron *89*, 857–866.

Prasad, J.A., and Chudasama, Y. (2013). Viral tracing identifies parallel disynaptic pathways to the hippocampus. J. Neurosci. *33*, 8494–8503.

Rodriguez-Raecke, R., Niemeier, A., Ihle, K., Ruether, W., and May, A. (2009). Brain gray matter decrease in chronic pain is the consequence and not the cause of pain. J. Neurosci. *29*, 13746–13750.

Samineni, V.K., Premkumar, L.S., and Faingold, C.L. (2017). Neuropathic pain-induced enhancement of spontaneous and pain-evoked neuronal activity in the periaqueductal gray that is attenuated by gabapentin. Pain *158*, 1241–1253.

Schulz, E., May, E.S., Postorino, M., Tiemann, L., Nickel, M.M., Witkovsky, V., Schmidt, P., Gross, J., and Ploner, M. (2015). Prefrontal gamma oscillations encode tonic pain in humans. Cereb. Cortex *25*, 4407–4414.

Seminowicz, D.A., Wideman, T.H., Naso, L., Hatami-Khoroushahi, Z., Fallatah, S., Ware, M.A., Jarzem, P., Bushnell, M.C., Shir, Y., Ouellet, J.A., and Stone, L.S. (2011). Effective treatment of chronic low back pain in humans reverses abnormal brain anatomy and function. J. Neurosci. *31*, 7540–7550.

Spellman, T., Rigotti, M., Ahmari, S.E., Fusi, S., Gogos, J.A., and Gordon, J.A. (2015). Hippocampal-prefrontal input supports spatial encoding in working memory. Nature *522*, 309–314.

Stagg, C.J., Lin, R.L., Mezue, M., Segerdahl, A., Kong, Y., Xie, J., and Tracey, I. (2013). Widespread modulation of cerebral perfusion induced during and after transcranial direct current stimulation applied to the left dorsolateral prefrontal cortex. J. Neurosci. *33*, 11425–11431.

Tappe-Theodor, A., and Kuner, R. (2014). Studying ongoing and spontaneous pain in rodents–challenges and opportunities. Eur. J. Neurosci. *39*, 1881–1890.

Taxidis, J., Coomber, B., Mason, R., and Owen, M. (2010). Assessing cortico-hippocampal functional connectivity under anesthesia and kainic acid using generalized partial directed coherence. Biol. Cybern. *102*, 327–340.

Vachon-Presseau, E., Tétreault, P., Petre, B., Huang, L., Berger, S.E., Torbey, S., Baria, A.T., Mansour, A.R., Hashmi, J.A., Griffith, J.W., et al. (2016). Corticolimbic anatomical characteristics predetermine risk for chronic pain. Brain *139*, 1958–1970.

Vertes, R.P., Hoover, W.B., Szigeti-Buck, K., and Leranth, C. (2007). Nucleus reuniens of the midline thalamus: link between the medial prefrontal cortex and the hippocampus. Brain Res. Bull. *71*, 601–609.

Walker, A.K., Kavelaars, A., Heijnen, C.J., and Dantzer, R. (2013). Neuroinflammation and comorbidity of pain and depression. Pharmacol. Rev. *66*, 80–101.

Williams, A.C.D.C., and Craig, K.D. (2016). Updating the definition of pain. Pain *157*, 2420–2423.

Wu, X.B., Liang, B., and Gao, Y.J. (2016). The increase of intrinsic excitability of layer V pyramidal cells in the prelimbic medial prefrontal cortex of adult mice after peripheral inflammation. Neurosci. Lett. *611*, 40–45.

Xu, Z.Z., Zhang, L., Liu, T., Park, J.Y., Berta, T., Yang, R., Serhan, C.N., and Ji, R.R. (2010). Resolvins RvE1 and RvD1 attenuate inflammatory pain via central and peripheral actions. Nat. Med. *16*, 592–597.

Yue, L., Ma, L.Y., Cui, S., Liu, F.Y., Yi, M., and Wan, Y. (2017). Brain-derived neurotrophic factor in the infralimbic cortex alleviates inflammatory pain. Neurosci. Lett. *655*, 7–13.

Zain, M., and Bonin, R.P. (2019). Alterations in evoked and spontaneous activity of dorsal horn wide dynamic range neurons in pathological pain: a systematic review and analysis. Pain *160*, 2199–2209.

Zhang, M., Liu, J., Zhou, M.M., Wu, H., Hou, Y., Li, Y.F., Yin, Y., Zheng, L., Cai, J., Liao, F.F., et al. (2017). Anxiolytic effects of hippocampal neurosteroids in normal and neuropathic rats with spared nerve injury. J. Neurochem. *141*, 137–150.

Zheng, J., Jiang, Y.Y., Xu, L.C., Ma, L.Y., Liu, F.Y., Cui, S., Cai, J., Liao, F.F., Wan, Y., and Yi, M. (2017). Adult hippocampal neurogenesis along the dorsoventral axis contributes differentially to environmental enrichment combined with voluntary exercise in alleviating chronic inflammatory pain in mice. J. Neurosci. *37*, 4145–4157.

STAR★METHODS

KEY RESOURCES TABLE

REAGENT or RESOURCE	SOURCE	IDENTIFIER
Antibodies		
Rabbit polyclonal anti-Cre	Abcam	Cat# ab190177
Alexa Fluor 488-conjugated goat anti-rabbit IgG	ZSGB-BIO	ZF-0511
Bacterial and Virus Strains		
pAAV-CaMKII-ChR2(H134R)-mCherry	OBIO Technology	AG26966
pAAV-CaMKII-mCherry	OBIO Technology	CN848
AAV5-CaMKII-hM3D(Gq)-mCherry	the University of North Carolina Vector Core Facilities	N/A
AAV5-CaMKII-hM4D(Gi)-mCherry	the University of North Carolina Vector Core Facilities	N/A
pAAV2-hSyn-Cre-GFP	Vigene Technology	N/A
pAAV2-CAG-DIO-BDNF-mCherry-3*flag	Vigene Technology	N/A
Chemicals, Peptides, and Recombinant Proteins		
Clozapine N-oxide	Tocris	4936/50
DAPI	Cell Signaling Technology	4083S
Complete Freund's adjuvant	Sigma-Aldrich	F5881-10ML
Ibuprofen	Sigma-Aldrich	I4883-1G, CAS:15687-27-1
Critical Commercial Assays		
BDNF Emax® ImmunoAssay System kit	Promega	Cat# G7610 RRID: AB_2571723
Experimental Models: Organisms/Strains		
Rats: Sprague-Dawley rats	Department of Laboratory Animal Sciences, Peking University Health Science Center	Cat# 5651135, RRID: MGI:5651135
Software and Algorithms		
MATLAB	MathWorks	RRID:SCR_001622
GraphPad Prism	GraphPad	RRID:SCR_002798
Smart	Panlab	RRID:SCR_002852
KlustaKwik	http://klustakwik.sourceforge.net/	RRID:SCR_014480
NeuroScope	http://www.nitrc.org/projects/neuroscope/	RRID:SCR_002455
NDManager	https://sourceforge.net/projects/ndmanager/	N/A

LEAD CONTACT AND MATERIALS AVAILABILITY

Further information and requests for resources and reagents should be directed to and will be fulfilled by the Lead Contact, Ming Yi (mingyi@hsc.pku.edu.cn). This study did not generate new unique reagents.

EXPERIMENTAL MODEL AND SUBJECT DETAILS

Animals

Adult male Sprague-Dawley rats (280–300 g at the beginning of experiments) were provided by the Department of Laboratory Animal Sciences, Peking University Health Science Center (Beijing, China). Rats were housed in 4–6 cohorts unless otherwise noted in a room temperature of ~23°C under 12–h dark-light cycle with free access to food and water. All experimental procedures were approved by the Animal Care and Use Committee of our University, according to the guidelines of the International Association for the Study of Pain.

CFA-induced inflammatory pain

Following our previous protocol (Fan et al., 2018; Yue et al., 2017), the rat was anesthetized with isoflurane. The plantar surface of left hindpaw was cleaned by 75% ethanol before a total of 100 μl complete Freund's adjuvant (CFA, Sigma-Aldrich, St Louis, USA) was injected intraplantarly to induce inflammatory pain. Control rats received injection of equal volumes of normal saline.

METHOD DETAILS

In vivo electrophysiology: surgery

For *in vivo* electrophysiological recording, electrode or optrode implantation for vCA1 and IL recording was based on a custom, 3D-printed design. For simultaneous IL and vCA1 recording, 15 stereotrodes of tungsten wires (20 μm in diameter, California Fine Wires Company) array with a microdrive were used for recording local field potential (LFP) and multi-unit activity in the IL (AP: +3.0 mm, ML: −0.5 mm, DV: −4.4 mm), and a non-moveable single tungsten wire (diameter 50 μm, California Fine Wires Company) was used for recording LFP in the vCA1 (AP: −5.5 mm, ML: −5.5 mm, DV: −5.5 mm). For the optrode, a stereotrode array combined with the LED optical fiber (200 μm in diameter, Newtoon, Hangzhou, China) was used for IL and the single electrode was used for vCA1 as described above. The impedance of stereotrode was between 1 to 1.5 MΩ, the impedance of single electrode was between 500 kΩ to 1 MΩ.

Independent cohorts of rats from behavioral tests were used for electrophysiological recording. The animals were initially anesthetized with isoflurane at 3% of the gas volume, which gradually decreased and stabilized at 1.0 to 1.5%. Once stably anesthetized, the animal was fitted with ear bars and mounted in the stereotaxic frame. Electrodes and optrodes were fixed on the skull by dental acrylic and protected by a custom, 3D-printed shell for the longitudinal recording. The reference and ground wires were set on the cerebellum.

After surgery, the rat was singly housed and allowed to recover for at least one week before further experiments.

In vivo electrophysiology: recording

After recovery from surgery, stereotrodes in the IL were slowly lowered to screen for spikes. After reaching a suitable position, the electrodes were stabilized without further movement.

The rat was allowed to move freely in a transparent plastic chamber (30 cm × 30 cm × 40 cm) with video recording. The chamber floor was a grid plate with stainless steel bars of 2 mm in diameter and 8 mm in between. Electrophysiology data were acquired using 32-channel Intan system (Intan Technologies, Los Angeles, USA). An electrode interface board was connected to a headstage, which was connected to the system amplifier with cables.

Electrophysiology recording was performed when the rat was quietly awake. Each recording session contained a 30-min resting phase, followed by a stimulation phase with 20 noxious laser stimuli. Laser stimulation was generated by an ultra-pulse carbon dioxide laser therapeutic machine (DM-300, Dimei, Changchun, China) and delivered to the left hindpaw (injected with CFA or normal saline.) of the recorded rat from the guide arm. The tip of the guide arm kept away from the plantar surface of the paw at a distance of 2 cm. The focus of laser beam was altered a little bit from trial to trial to avoid possible tissue damage. The laser power ranged from 2 to 4 W with an emission time of 20 ms. The power used for each rat was the lowest power to induce >8 trials with paw lifting behavior in 10 laser stimuli, determined by a pilot experiment before formal recording. The trials without paw-lifting behavior were excluded from further analysis. The interstimulus interval was no less than 60 s to avoid hyperalgesia. Six recording sessions were conducted for each rat 1 day before (baseline) and 1, 3, 6, 9 and 12 days after CFA injection. Electrode position was confirmed with Nissl staining after all recording sessions.

For administration of ibuprofen, ibuprofen (Sigma-Aldrich) was dissolved in 1% carboxymethylcellulose before administration, and administered by oral gavage at a dose of 10 mg/kg on CFA d 3. Thirty-minute *in vivo* recording was performed before (as ''Before'' in Figure 5) and 30 min after administration (as ''After'' in Figure 5).

Electrophysiological data analysis: data preprocessing

To extract LFPs, raw data were down-sampled to 1250 Hz, low-pass filtered at 200 Hz and notch-filtered between 48 and 52 Hz. Channels with noise contamination were excluded artificially. LFP-related analysis (PSD, PAC and PDC) was averaged from each channel or each channel pair (each IL channel with the single vCA1 channel).

To measure spiking activity of single units, electrophysiological data were collected from the microwires and high-pass filtered at 300 Hz. Time intervals where the amplitude variance exceeded 2 standard deviations were considered to contain multi-unit activity. The time intervals were subsequently decomposed using a principal component analysis, and single-unit activity was sorted automatically using KlustaKwik followed by manual adjustment using the software Klusters.

Electrophysiological data analysis: spike classification

Spike sorting was carried out in KlustaKwik (http://klustakwik.sourceforge.net/). Using principal component analysis, a rough separation of units from pyramidal neurons and interneurons in the IL was mainly based on spike wave shape and mean baseline firing rate: putative interneurons had a high firing rate (> 10 Hz) and a narrow peak-to-valley width (< 0.4 ms), whereas putative pyramidal neurons showed a lower mean firing rate (< 10 Hz) and a wide peak-to-valley width (> 0.5 ms) (Barthó et al., 2004).

Electrophysiological data analysis: power spectral density

For power spectral density, LFP signals of vCA1 and IL recorded during a resting condition were fragmented into 40 s segments and analyzed by mtspectrumsegc.m in Chronux toolbox (http://chronux.org). The bandwidth product was 3, and 5 tapers were used. To avoid power noise, the signals were notch filtered at 50 Hz. The power spectral density was divided into six frequency bands: delta (1–4 Hz), theta (4–8 Hz), alpha (8–13 Hz), beta (13–30 Hz), low gamma (30–50 Hz) and high gamma (50–100 Hz).

Electrophysiological data analysis: partial directed coherence

Generalized partial directed coherence (gPDC) was calculated as previously described (Baccalá and Sameshima, 2001; Taxidis et al., 2010). This algorithm was based on a multi-variate autoregressive (MVAR) model, which integrated both vCA1 and IL signals.

In brief, the two different time series were modeled as a form:

$$\begin{bmatrix} x_1(t) \\ x_2(t) \end{bmatrix} = \sum_{r=1}^{p} Ar \left(\begin{bmatrix} x_1(t-r) \\ x_2(t-r) \end{bmatrix} \right) + \begin{bmatrix} u_1(t) \\ u_2(t) \end{bmatrix}$$

[(u1(t), u2(t)] represented uncorrelated Gaussian white noise processes representing the model residuals, the model order p was determined by the minimum of Akaike Information Criterion or Bayesian Information Criterion. The gPDC was defined as follows:

$$\left| C_{i \leftarrow j}(f) \right| = \frac{a_{ij}(f)}{\sqrt{\sum_k \frac{1}{\sigma_k^2} \left| a_{kj}(f) \right|^2}}$$

$A_{ij}(f)$ was the Fourier transformation of the MVAR coefficient $\left(Ar = \begin{bmatrix} a_{11} & a_{12} \\ a_{21} & a_{22} \end{bmatrix} \right)$, σ_k represented the standard deviation of the model residuals. The gPDC value was in the interval of [0 1], where "0" stood for the absence of an influence of a target on the source and "1" stood for a linearly predictable target from the source. In the present study, the PDC value was averaged across the entire frequency spectrum for quantitative analysis.

Electrophysiological data analysis: phase amplitude coherence

To estimate cross-frequency coupling between vCA1 and IL, we adopted the method presented by Canolty et al. (2006). We constructed a composite complex-valued signal by combining the amplitude time series of the IL at the frequency band (15-100 Hz, 5Hz steps with 4Hz bandwidth) with the phase time series of the vCA1 at the frequency band (2-20 Hz, 1Hz steps with 1Hz bandwidth):

$$z(t) = \text{amplitude}(t) \times e^{i \times phase(t)}$$

The instantaneous amplitude and phase were generated by Hilbert transform of the filtered time series. The mean of z(t), M_{raw} was normalized to a set of surrogate means M_{surr}, which were created by offsetting amplitude(t) and phase(t) by randomized time lag, and the composite signal was a function of both time and lag:

$$z(t, \tau) = \text{amplitude}(t + \tau) \times e^{i \times phase(t)}$$

A population of 200 surrogate signals were created and compared to the original signal to generate a distribution of modulation index:

$$M_{NORM} = \frac{M_{RAW} - \mu}{\sigma}$$

where μ was the mean of the M_{surr} distribution and σ was the standard deviation of the M_{surr} distribution.

PAC value was calculated by the combination of theta phase (4-8 Hz) of the vCA1 and high gamma amplitude (70-90 Hz) of the IL.

Electrophysiological data analysis: spectrogram

To calculate the time-frequency spectrogram of the IL during laser stimuli, we used Gabor wavelet and the spectrum was normalized to baseline (0.5 s before laser onset) for each trial. The spectrum at 1 s after laser onset was averaged in both theta and gamma bands, for comparison between different stages of inflammatory pain.

Electrophysiological data analysis: neuronal response to laser stimuli

To measure neuronal responses to laser stimuli, the firing rate was calculated at the period that 1 s before and 1 s after laser onset in each trial. Paired t test was performed to compare the firing rate before and after laser onset, and responses were divided into excitatory (increased firing rate with p value < 0.05), inhibitory (decreased firing rate with p value < 0.05) or neutral (p value > 0.05) responses. The extent of firing variation was defined by the index as followed:

$$\text{index} = \left| \frac{F_{after} - F_{before}}{F_{after} + F_{before}} \right|$$

To calculate the mean firing rate of the units pre- and post CNO administration, the spikes were binned into 30 s and the mean firing rate was normalized by using Z-score to the baseline (30 min before the CNO administration). The units with the mean Z scores of the 30 min after the CNO administration exceeding to 1.98 ($p < 0.05$) were defined as the neuron with increased firing rates.

Electrophysiological data analysis: phase locking

To establish whether the spike firing was concentrated at a certain phase of the LFP, the distribution of instantaneous phases when each spike firing was calculated and displayed in the form of a rose plot. To assess nociception-related phase-locking, we analyzed the data 1 s after laser onset among all trials of each recorded neuron. The phase interval from $-\pi$ to π was uniformly divided into 16 bins and the number of spikes in each phase interval was counted. The spike-LFP phase vector was computed to indicate the locked phase and intensity. The Rayleigh Z test was performed by CircStat toolbox to determine the significance of phase-locking. Since the Rayleigh Z test was sensitive to sample size, the statistic was calculated from the instantaneous phases of the same number of spikes (40 spikes in this case) which were randomly chosen among all trials of each recorded neuron. Neurons with spikes fewer than 40 were excluded from following proportion comparison. Pyramidal neurons phase-locked to hippocampal theta frequency were categorized when $p < 0.05$ of Rayleigh Z test. The mean resultant length was the sum of vector values and calculated in the phase-locking neurons.

Behavioral test: spontaneous paw lifting

Each rat was handled by the experimenter for 10 min/day for three consecutive days before behavioral testing. Experimenters were blind from animal grouping.

Spontaneous nociceptive behavior was measured 1 day before and 1, 3, 6, 9 and 12 days after CFA injection. Rats were placed in a transparent plastic chamber (30 cm × 30 cm × 30 cm) and video-recorded for 30 min. CFA-induced spontaneous nociceptive behavior was analyzed by counting the time spent on lifting, licking, and flinching of the injected hindpaw in this 30 min period (Djouhri et al., 2006; Lee et al., 2018).

Behavioral test: conditioned place preference (CPP)

The CPP apparatus was a three-chamber box with a middle chamber (10 cm × 30 cm × 30 cm) which could be opened or closed off to either of two end chambers (30 cm × 30 cm × 30 cm). The two end-chambers were differentiated by distinct visual and tactile features (King et al., 2009; LeBlanc et al., 2016).

During the preconditioning session (day 2 or day 8 post-CFA injection), the rats were released from the middle chamber to freely explore the apparatus for 15 min. Time spent in each chamber was recorded. Rats were excluded if they spent more than 70% of the time (> 630 s) in any one chamber.

During the conditioning session (days 3–6 or days 9–12 post-CFA injection), rats underwent "pairing" where they were individually restricted to one end chamber after receiving vehicle injection for 30 min in the morning. Four hours after vehicle injection, they were restricted to the other end chamber for 30 min after receiving CNO (see below "chemogenetics") or morphine (2.5 mg/ml dissolved in sterile saline, 2.5 mg/kg, *s.c.*, First Pharmaceutical Factory of Qinghai, China) injection (Hung et al., 2015). Chamber pairing was counterbalanced in different rats.

On the following test day (day 7 or day 13 post-CFA injection), rats were released from the middle chamber and allowed to explore all chambers for 15 min.

CPP score was calculated as followed:

$$\text{CPP score} = \frac{\text{T test} - \text{T preconditioning}}{\text{T preconditioning}} \times 100\%$$

t test was the time in the drug-paired chamber on the test day. T preconditioning represented the time in the drug-paired chamber on the preconditioning day.

Behavioral test: evoked nociceptive responses

Each rat was adapted in a plexiglas box for 30 min per day for three consecutive days before measurement. Thermal or mechanical pain thresholds were measured 1 day before and 1, 3, 6, 9, 12, 18, 24 and 30 days after CFA injection, while the rat stayed calm and awake.

For thermal nociceptive response, paw withdrawal latencies (PWLs) were measured by a focused radiant heat (40 W of power) applied to either hindpaw (Hargreaves Method, IITC 390). PWLs were recorded three times and averaged as the thermal pain threshold. A cut-off value of 30 s was set to avoid possible tissue injury (Fan et al., 2018).

For mechanical nociceptive response, fifty percent paw withdrawal thresholds (50% PWTs) were measured by *von* Frey hairs (0.41 to 15.1 g; North Coast, Gilroy, CA, USA) applied to the central plantar surface of either hindpaw. The 50% PWTs were calculated by the "up and down" method as described earlier (Fan et al., 2018).

Behavioral test: open field test

The apparatus was a 100 cm × 100 cm × 50 cm box (Shanghai Mobiledatum Information Technology Co., Shanghai, China) in a quiet and 30 lux illuminated room. Each rat was placed in the central area and video-recorded for 5 min. Time spent (C.Time) and number of entries (C.Dis) in the central area (60 × 60 cm) and total distance traveled (T.Dis) in the field were measured using the SMART software (version 2.5.21, Panlab, SMART Video tracking, Harvard Apparatus). The field was cleaned by 75% ethanol between tests (Zhang et al., 2017).

Behavioral test: elevated plus-maze test

The elevated plus-maze test was performed on the next day of the open field test, unless otherwise noted. The maze (Shanghai Mobiledatum Information Technology Co., Shanghai, China) was placed 50 cm above the floor in a 30-lux illuminated room and consisted of two open arms and two closed arms (48 cm × 8 cm and 40 cm wall height for the closed arms). Each rat was placed onto the central area, heading toward the same open arm, and videotaped in the following 5 min. Time spent (O.Time) and numbers of entries (O.Entries) into open arms and total arm entries (T.Entries) were analyzed using the SMART software. The maze was cleaned by 75% ethanol between tests (Zhang et al., 2017).

Optogenetics

Vector viruses used for optogenetics (AAV5-CaMKIIα-ChR2-mCherry and AAV5-CaMKIIα-mCherry, 1.4×10^{13} virus particles/ml) were packaged and purchased from OBIO Technology (Shanghai, China). The rat was anesthetized with 1% sodium pentobarbital (0.1g/kg, *i.p.*) and positioned in a stereotaxic frame (RWD, Shenzhen, China). The virus solution was injected bilaterally into vCA1 (AP −5.0/5.5 mm; ML ± 5.5 mm from bregma; DV −5.5 mm from brain surface) with 0.5 μl/hole, 2 holes/side, at a speed of 0.1 μl/min. After injection, needles were left *in situ* for an additional 5 min. Behavioral tests and electrophysiology recording were performed 8 weeks after virus injection.

An optogenetic system (PlexBright LED, Plexon, Hong Kong) was used for ChR2 activation. The light was produced by the implanted LED fiber using a 200-mA current input. The 470-nm blue light was delivered at 6–8 mW, 20 Hz in a square wave stimulation mode (3-ms pulse, 1 s on, 2 s off).

Chemogenetics

For cannula implantation, the rat was anesthetized with 1% sodium pentobarbital (0.10 g/kg, *i.p.*) and positioned in a stereotaxic frame (RWD, Shenzhen, China). A guide cannula (O.D. 0.48 mm/I.D. 0.34 mm, C.C 1.2 mm, RWD, Shenzhen, China) was bilaterally implanted 1.5 mm above IL (AP: +3.0 mm, ML: ± 0.5 mm, DV: −4.4 mm). The cannula was secured with four screws and dental acrylic cement on the skull. The matching cap (0.5 mm below the guide cannula, RWD, Shenzhen, China) was inserted into the guide cannula to prevent clogging.

For chemogenetics, AAV5-CaMKIIα-hM3D(Gq)/hM4D(Gi)-mCherry and AAV5-CaMKIIα-mCherry (1×10^{12} virus particles/ml) were packaged and purchased from the University of North Carolina Vector Core Facilities, USA. Virus injection followed procedures similar to the optogenetics experiment. Behavioral tests and electrophysiology recording were performed 8 weeks after virus injection.

Clozapine *N*-oxide (CNO; Tocris, Bristol, UK) was dissolved in artificial cerebrospinal fluid at a concentration of 0.8 mM (Fan et al., 2018; Mahler et al., 2014). A volume of 0.5 μL per hemisphere was microinjected into the IL over a 5 min period using the polyethylene catheter (PE-10) connected to a 1 μL syringe needle (RWD, Shenzhen, China). The needle was kept for 5 min to maximize drug diffusion. Behavioral tests started 30 min after drug injection.

BDNF overexpression

For BDNF overexpression, pAAV2-hSyn-Cre-GFP (AAV2-Retro) (0.5 μl/side, Vigene Technology, Shandong, China) was injected into bilateral IL (AP +3.0 mm; ML ± 0.5 mm from bregma; DV −4.4 mm from brain surface). pAAV2-CAG-DIO-BDNF-mCherry-3*flag was injected into bilateral vCA1 as described above. A viral vector without BDNF gene insertion was used as controls. Behavioral tests and electrophysiology recording were performed 6 weeks after virus injection.

Histology

The rat was deeply anesthetized with 1% sodium pentobarbital (0.1g/kg, *i.p.*) and perfused intracardially with 0.9% saline followed by 4% paraformaldehyde (PFA, in 0.1 M phosphate buffer, pH 7.4). The isolated brain was post-fixed with 4% PFA for 12 h, and cryoprotected in 20% and 30% sucrose solutions in turn. The fixed brain was cut into 50-μm thick slices for identifying electrode tracks and 30-μm thick slices for immunostaining.

Recording sites were identified by visual examination of electrolytic lesions, which were induced immediately before perfusion by passing currents (2 mA, 15 s) through an electrode at each implantation site. The brain slices were stained with Nissl and photographed by light microscope (Leica DMI 4000B, Wetzlar, Germany).

Virus infection was confirmed after behavioral tests by detecting fluorescin using a fluorescence microscope (Leica DMI 4000B, Wetzlar, Germany).

For Cre immunostaining, free-floating sections were washed in the phosphate buffered saline (PBS), blocked with a buffer containing 3% bull serum albumin and 0.3% Triton X-100 for 1 h, and incubated with the following primary antibodies in 4°C for 24 h: rabbit anti-Cre antibody (1:500, ab190177, Abcam). Sections were washed in PBS and incubated with secondary antibody at room temperature for 90 min: Alexa Fluor 488-conjugated goat anti-rabbit IgG (1:500, ZF-0511, ZSGB-BIO).

ELISA for BDNF measurement

After anesthesia, the rat brain was removed immediately from the skull and placed on a filter paper containing cold normal saline, over a glass plate filled with crushed ice. Bilateral IL and vCA1 tissues were dissected and homogenized in ice-cold lysis buffer containing protease inhibitor cocktail. The homogenate was centrifuged at 10,000 × g for 10 min at 4°C. BDNF level were measured with ELISA method using the BDNF Emax® ImmunoAssay System kit (Promega, WI, USA) according to the manufacturer's instructions. The absorbance of samples was read at 450 nm by a microplate reader (23227, Thermo Fisher Scientific) and values calculated according to related standard curves. Total protein concentrations in the sample were determined using a BCA protein assay kit. Measurements were performed in duplicate. Data were presented as a ratio between BDNF and total protein level.

QUANTIFICATION AND STATISTICAL ANALYSIS

Data were expressed as mean ± SEM. Group comparisons were made using either one-way or two-way analysis of variance (ANOVA) followed by Bonferroni post hoc tests. Single variable comparisons were made with two-tail unpaired Student's t test. Chi-square analyses or Fisher's exact test were used to compare proportions. Mann-Whitney tests or Wilcoxon signed-rank tests were used to compare *in vivo* neural firing rates. Friedman test was used in the comparisons of three or more groups with abnormal distribution. All statistics were calculated using GraphPad Prism 6 software or MATLAB. $p < 0.05$ was taken as statistically significant.

DATA AND CODE AVAILABILITY

The datasets and code supporting the current study have not been deposited in a public repository because all data are presented in the main text and in Supplementary Figures and Tables, but are available from the corresponding author on request.